Cradle-to-Gate Life Cycle Assessment of Multi-Jet Fusion 3D Printing

By
Michael B. London

A thesis submitted in partial
fulfillment of the requirements for the
degree of Master of Science
(Environment and Sustainability) at
the University of Michigan

April 2020

Thesis Committee:
Geoffrey Lewis, Ph.D., Center for Sustainable Systems Research Specialist
Gregory Keoleian, Ph.D., Center for Sustainable Systems Director

Acknowledgements

I would like to express my utmost gratitude to my thesis advisors, Dr. Geoffrey Lewis and Dr. Gregory Keoleian, for their invaluable guidance, wisdom, support, and patience throughout this journey. I am especially indebted to Dr. Lewis for his expert counsel, constant encouragement, and many hours of dedicated mentorship. Dr. Lewis helped me hone my research skills and stay the course amidst the rabbit holes I frequently encountered. I owe the original inspiration of this thesis to Dr. Keoleian, who introduced me to the world of life cycle assessments with his Sustainable Energy Systems and Industrial Ecology courses. Dr. Keoleian's advocacy and generosity to advise amongst his many competing priorities gave me the motivation to take on this challenge. The personal and professional learnings I gained from Dr. Lewis and Dr. Keoleian will stick with me for a lifetime.

I would also like to thank Dr. H. Thomas Etheridge and David Woodlock from HP Inc., and Lise Laurin from Earthshift Global, LLC, for their responsive communication and constructive engagement with this research. Their assistance enhanced the accuracy, relevance, and importance of this work.

Finally, I would like to thank my family for their countless words of enthusiasm for my goals and confidence in my abilities. Furthermore, this work would not have been possible without the uplifting support and thoughtful care of my wife, Leslie. Her tireless efforts and myriad sacrifices while working and caring for our son, our pets, and our home afforded me the time and energy to complete this research. I am so fortunate and grateful to be her partner.

Abstract

The rapid pace of growth in additive manufacturing has left significant knowledge gaps in life cycle assessment (LCA) literature, limiting inclusion of sustainability considerations in manufacturing and supply chain decisions. The recent introduction of HP's Multi-Jet Fusion (MJF) 3D printing technology shows promise as an alternative to other additive and conventional manufacturing methods on the market; however, scarce environmental assessments of MJF exist in publicly available literature. This study fills the gap in current additive manufacturing LCAs to improve decision-making in plastic part manufacturing. This assessment investigated the cradle-to-gate life cycle energy consumption and greenhouse gas (GHG) emissions of HP's MJF 3D printing technology in comparison to injection molding across production quantities ranging from 100 to 100,000 parts for a plastic product. This analysis leveraged secondary data from various sources, including MJF technical documents, communications with HP representatives, published LCA literature, the ecoinvent 3.5 database, and Argonne National Laboratory's Greenhouse Gases, Regulation Emissions, and Energy Use in Transportation (GREET) 2019 model. Results of the analysis indicate that MJF 3D printing technology emits less GHG emissions than injection molding with aluminum or steel tooling at quantities up to about 450 and 800 parts, which is 5 to 8 prints jobs for the studied design. 3D printing electricity consumption and material yield are the major factors contributing to MJF's GHG emissions. Varying the manufacturing facility electricity generation source, post processing time, raw material production life cycle inventory data, and printing speed can substantially alter the GHG emissions breakeven point between MJF and injection molding. Optimum conditions of these variables for MJF could shift the GHG emissions breakeven with injection molding to a point between 5,000 to 10,000 parts. MJF's lower material yield and requirement for fusing and detailing agent ultimately limit the GHG emissions breakeven quantity with injection molding. Consequently, MJF's GHG emissions breakeven quantity with injection molding remains one to two orders of magnitude lower than HP's advertised economic breakeven quantity of 110,000 parts. This study also shows that MJF is slightly more energy efficient and more resource efficient than selective laser sintering, MJF's peer additive manufacturing process.

Table of Contents

List of Tables

List of Figures

1. Introduction

1.1. Background

Advancing the reduction of greenhouse gas (GHG) emissions from industry is a major challenge for both public policymakers and business leaders (Fischedick et al., 2014). In 2018, industry was the largest contributor to U.S. GHG emissions, accounting for 29.1% of emissions (U.S. Environmental Protection Agency, 2020). This study examines additive manufacturing, one of the many promoted approaches to fostering greater environmental sustainability in industry (Ford & Despeisse, 2016; Mani, Lyons, & Gupta, 2014).

As defined by ISO/ASTM 52900, additive manufacturing is a "process of joining materials to make parts from 3D model data, usually layer upon layer," as opposed to conventional manufacturing methods (ASTM International, 2015). Conventional manufacturing methods include subtractive shaping and formative shaping (ASTM International, 2015). Examples of subtractive shaping processes include milling, drilling, turning, and electric discharge machining (EDM) (ASTM International, 2015). Formative shaping includes forging, casting, bending, and injection molding processes, which produce the desired shape by applying pressure to a body of material (ASTM International, 2015).

Advocates of additive manufacturing, commonly referred to as "3D printing," promote the process as an alternative to conventional manufacturing based on several known advantages, including greater design freedom, rapid production of small batches at relatively low cost, and avoidance of tooling (Gutowski et al., 2017; Huang, Leu, Mazumder, & Donmez, 2015; Kellens, Baumers, et al., 2017; Mansour & Hague, 2003; Tuck, Hague, Ruffo, Ransley, & Adams, 2008).[1] The design freedom afforded by additive manufacturing enables the production of complex part designs that would be more difficult or impossible to produce with conventional manufacturing methods (Gutowski et al., 2017; Kellens, Baumers, et al., 2017; Mansour & Hague, 2003). On the other hand, recognized disadvantages of additive manufacturing include slow process times, poor surface quality, and inferior dimensional tolerances (Gutowski et al., 2017; Kellens, Baumers, et al., 2017).

Notwithstanding the economic and engineering characterizations of additive manufacturing, studies on this emerging industry posit that additive manufacturing brings substantial environmental benefits to supply chains. Chen et al. (2015) suggests that additive manufacturing can reduce carbon footprints by reducing raw material consumption, eliminating the need for energy intensive processes associated with tooling production, and reducing energy demand for transportation of products that could be otherwise manufactured closer to the consumer. Ford and Despeisse (2016) identified four major categories of sustainability benefits from additive manufacturing: product and process redesign; material input processing; make-to-order component and product manufacturing; and closing the loop. Among these categories, examples of sustainability benefits arising from additive manufacturing included simplified assemblies, reduced material inputs, reduced waste generation, vehicle and aircraft light weighting, and reduced energy intensity (Ford & Despeisse, 2016).

[1] This paper uses additive manufacturing and 3D printing interchangeably.

Recognition of the new opportunities afforded by additive manufacturing for value creation have spurred rapid growth in the industry. The number of enterprises involved in the manufacturing of devices for additive manufacturing, herein referred to as "3D printers," will have grown at an annualized rate of 35.4% from 2014 to 2019 (Heikoff, 2019). Industry research estimates the total revenue for manufacturers of 3D printers to be $4.5 billion in 2019 with expected growth to $8.5 billion in 2024 (Heikoff, 2019).

The rapid pace of growth in the additive manufacturing industry has left significant knowledge gaps in sustainability literature (Rejeski, Zhao, & Huang, 2018). Some additive manufacturing technologies have had little or no assessment of their environmental impacts (Kellens, Baumers, et al., 2017). Consequently, business leaders are left to consider manufacturing, procurement, and capital investment decisions without sufficient knowledge of the sustainability tradeoffs.

Introduced in 2016, HP Inc.'s Multi-Jet Fusion (MJF) 3D printing technology has received scarce environmental evaluation. However, industry adoption of MJF is markedly increasing (Back, 2019). The technology is 5 to 10 times faster than other 3D printing technologies (Stratasys Direct Manufacturing Inc., n.d.; Xu, Wang, Wu, Ananth, & Bai, 2019). In their evaluation of the mechanical performance of HP MJF printed parts, O'Connor, Dickson, and Dowling (2018) concluded that MJF exhibits "enormous potential to facilitate the wider adoption of 3D printing in a production environment" (p. 387). Moreover, MJF technology presents a potential alternative to conventional manufacturing for industrial-scale production volumes, which have been cost prohibitive for other additive manufacturing processes, such as selective laser sintering and fused deposition modeling (Minetola & Eyers, 2018; Ruffo, Tuck, & Hague, 2006). HP claims the technology enables large-scale 3D production, resulting in an economic breakeven point at 110,000 parts with injection molding and 65% lower cost than other additive manufacturing methods (Davies, 2017; HP Development Company L.P., 2017a). HP also announced the production of 10 million parts with its technology over the course of a year-long period (HP Development Company L.P., 2019d). Recognizing the economic and functional benefits of MJF, Smile Direct Club, a provider of clear aligner orthodontic therapy, recently installed 49 HP Jet Fusion 3D Printers in their facility to produce nearly 20 million mouth molds over the course of 12 months (HP Development Company L.P., 2019a).

1.2. Research Objective

This study seeks to fill the gap in additive manufacturing sustainability literature by investigating MJF 3D printing technology. The research objective of this study is to evaluate the life cycle primary energy consumption and GHG emissions of the HP MJF 4210 3D Printing system in relation to conventional manufacturing methods across different production volume scenarios.

1.3. Multi-Jet Fusion

MJF is considered a powder bed fusion (PBF) process technology, which ISO/ASTM 52900 defines as an "additive manufacturing process in which thermal energy selectively fuses regions of a powder bed" (ASTM International, 2015). The MJF process builds parts layer-by-layer over the working area of a build platform inside an HP Jet Fusion 3D built unit, depositing chemical agents onto select areas of each powder layer, and fusing those areas with infrared radiation (HP Development Company L.P., 2018c). **Figure 1** presents an overview of the MJF 3D printing process.

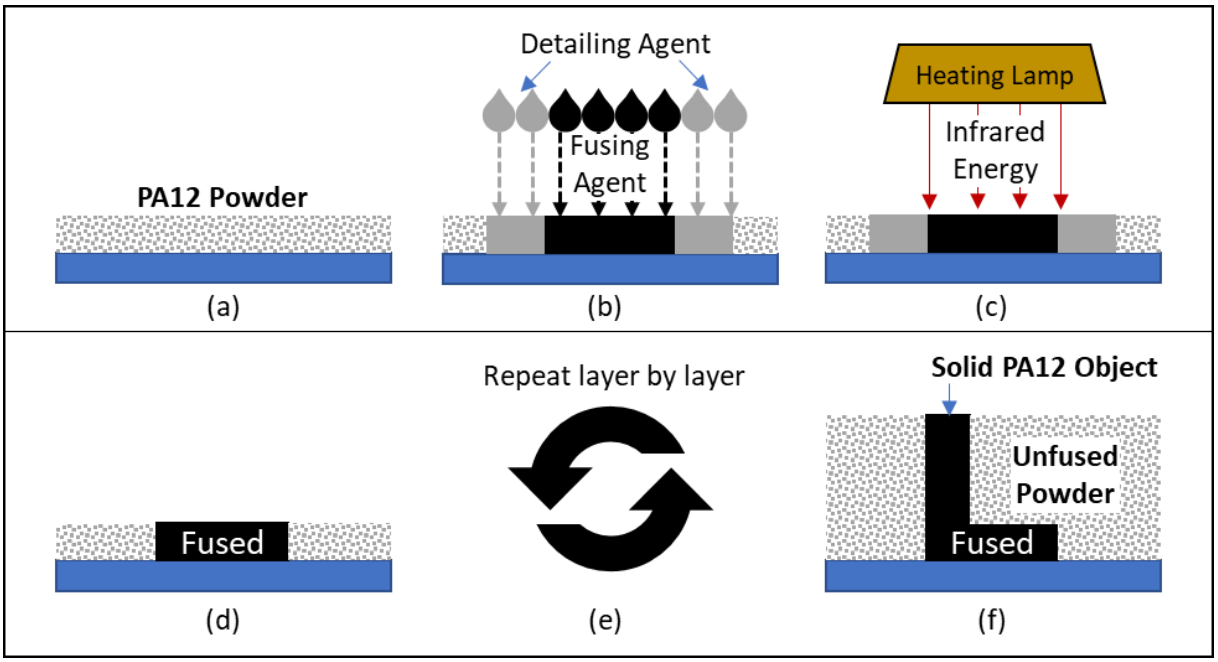

Figure 1. Overview of MJF 3D printing process. Adapted from HP MJF technology technical white paper (HP Development Company L.P., 2018c). General sequence of the MJF 3D printing process: (a) the printer spreads a layer of PA12 (or other material) powder over the working area of the build unit or a previous layer of powder; (b) fusing agent and detailing agent are deposited onto select areas of the powder layer; (c) infrared radiation fuses the areas where fusing agent was deposited; (d) the layer consists of fused and unfused powder; (e) steps (a) through (d) are repeated until object build completion; (f) at build completion, a fused object remains in a chamber of unfused powder for subsequent cooling, unpacking, and post-processing.

1.4. Literature Review

Despite the increasing adoption of MJF, only one LCA study exists in publicly available literature on the process. Tagliaferri, Trovalusci, Guarino, and Venettacci (2019) compared the production costs and environmental impact associated with three additive manufacturing technologies: fused deposition modeling (FDM), selective laser sintering (SLS), and MJF. Using the Eco-Indicator 99 method in SimaPro v7.1 software, the authors concluded that the MJF system had a lower environmental impact than both of the SLS and FDM systems evaluated (Tagliaferri et al., 2019). However, the description of methods, sources, and assumptions in this study, including the system boundary, process flow, life cycle inventory, and material yield, lack sufficient detail to thoroughly probe the results and facilitate their replication. Moreover, this study does not evaluate the MJF process' environmental impact in the context of conventional manufacturing methods.

In the absence of published LCA studies on MJF, existing literature on SLS provide a basis for the methods used in this paper. SLS serves as an appropriate additive manufacturing technology to benchmark MJF 3D printing against because SLS is also a powder-bed fusion technology and uses similar input materials (O'Connor et al., 2018). The main differences between the two additive manufacturing processes involve: (1) MJF uses fusing agents and detailing agents to

facilitate the fusing of selected powder regions while SLS does not use any additional agent; (2) MJF uses infrared radiation from a heating lamp while SLS uses directed laser energy (Bain, 2019; Ligon, Liska, Stampfl, Gurr, & Mülhaupt, 2017).

1.4.1. Raw Materials

MJF and SLS use similar raw material powders for part manufacturing, such as polyamide 11 (PA11) and polyamide 12 (PA12) (Ligon et al., 2017; Xu et al., 2019). PA12 is the most commonly used material for both MJF and SLS (Goodridge, Tuck, & Hague, 2012; Xu et al., 2019). However, previous LCAs on additive manufacturing with SLS used life cycle inventory (LCI) data for polyamide 6 (PA6) as modeling inputs for raw materials (Karel Kellens, Renaldi, Dewulf, Kruth, & Duflou, 2014; Telenko & Seepersad, 2010, 2012). The two polyamides have a similar molecular structure, but PA6 is less suitable for powder bed fusion than PA12 due to its higher melting point and higher viscosity (Kruth, Levy, Klocke, & Childs, 2007; Ligon et al., 2017). PA6 and PA12 also use different monomers for commercial manufacturing: caprolactam for PA6 and laurolactam for PA12 (Weber, 2011). Although crude oil and natural gas serve as the raw materials for both monomers, the production routes for the monomers differ. The common use of hydrolytic ring-opening polymerization to produce both monomers served as the primary justification for approximating the PA12 LCI with PA6 LCI data in prior LCA studies (Telenko & Seepersad, 2010).

1.4.2. Process Energy Consumption

Most environmental studies of SLS investigated specific energy consumption (SEC), which is the site energy consumed by the machine for production of 1 kilogram of product. In this context, SEC studies evaluated the energy efficiency of the SLS machine during the additive manufacturing process and did not include upstream energy generation, transmission, and distribution in their assessment of energy consumption. SEC values ranged from 51 MJ/kg to 237.68 MJ/kg (Baumers, Tuck, Bourell, Sreenivasan, & Hague, 2011; Kellens et al., 2011; Luo, Ji, Leu, & Caudill, 1999; Sreenivasan & Bourell, 2009). The methods for obtaining these SEC values varied significantly among the studies. Luo, Ji, Leu, and Caudill (1999) determined the SEC of two SLS machines based on the specifications from the machine equipment manufacturer and the specific gravity for polymer. The low end of the SEC range – 51 MJ/kg – was determined by measuring the average power consumption of an SLS system over the course of two builds and applying the observed value to a parametric model based on the specifications of the machine (Sreenivasan & Bourell, 2009). Kellens et al. (2011) measured power consumption for three SLS machines and conducted time studies across 86 batches of products with different polyamide materials to determine SEC values ranging from 94.7 MJ/kg to 143.3 MJ/kg. Kellens et al. (2011) concluded with an SLS LCA case study for a sample batch resulting in an SEC of 130.1 MJ/kg. Baumers et al. (2011) determined SEC values ranging from 204.31 MJ/kg to 237.68 MJ/kg by monitoring the power consumption of two machines during separate builds of two large prosthetic parts. In comparison to the lower SEC values from Kellens et al. (2011), Baumers et al. (2011) suggested that the higher SEC values observed in their experiments could be potentially attributed to a lower capacity utilization and longer process time, which may result from a smaller layer thickness and taller build height. Energy consumption values also vary as a result of part orientation and nesting efficiency (Baumers, Tuck, Wildman, Ashcroft, & Hague, 2011; Kellens et al., 2011; Kellens et al., 2014). Kellens et al. (2014) defines weight-based nesting efficiency as the weight of the parts being built divided

by the total weight of powder in the 3D printer chamber. A volume-based nesting efficiency, also referred to as packing density or build utilization factor, is the total volume of the parts divided by the total volume in the chamber (Dotchev & Yusoff, 2009). Kellens et al. (2014) developed a parametric model depicting significant potential for environmental impact reduction as a result of increased nesting efficiency. In their study, Baumers, Tuck, Wildman, et al., (2011) refer to packing density as capacity utilization and show that higher capacity utilizations for SLS machines result in a reduction of SEC.

Prior literature on the energy consumption of SLS provides a foundation for investigating MJF, but leaves out important steps of the production process for precise comparison. Existing studies of SLS do not assess the energy consumption associated with powder handling before the build or unpacking, powder recycling, cooling, and post-processing after the build (Gutowski et al., 2017; Kellens, Baumers, et al., 2017). However, these are non-trivial time and energy consuming steps of the manufacturing workflow for evaluation of an industrial-scale production process (Dotchev & Yusoff, 2009; Kellens, Baumers, et al., 2017). Current SLS and MJF systems include machines that provide powder mixing, loading, and unpacking functions (Dotchev & Yusoff, 2009; EOS GmbH Electro Optical Systems, n.d.; HP Development Company L.P., n.d.; Sintratec AG, n.d.). Moreover, most post-processing methods utilize compressed air systems, which consume substantial amounts of energy due to their low efficiency (Butler, 2011; Marshall et al., 2016).

1.4.3. Process Emissions

No publicly available studies have evaluated the direct air, soil, or water emissions of SLS additive manufacturing, signifying an important research need for the scientific community (Bours, Adzima, Gladwin, Cabral, & Mau, 2017; Kellens, Baumers, et al., 2017; Short, Sirinterlikci, Badger, & Artieri, 2015). Instead, several sustainability-related studies of SLS modeled indirect emissions using LCA software and different calculation methods, such as the Eco-Indicator 99 method to determine life cycle impacts of the process (Kellens et al., 2014; Luo et al., 1999; Sreenivasan & Bourell, 2009; Tagliaferri et al., 2019).

1.4.4. Resource Consumption

Most sustainability-related studies of SLS did not evaluate resource consumption using a LCA framework (Kellens, Mertens, Paraskevas, Dewulf, & Duflou, 2017). The studies that have examined resource consumption indicate a significant amount of waste generated by the SLS process, contradicting the often claimed benefit that additive manufacturing reduces material waste (Dotchev & Yusoff, 2009; Hopkinson, Hague, & Dickens, 2006; Kellens et al., 2014; Telenko & Seepersad, 2010). Telenko and Seepersad (2010) estimated that yields for SLS were likely to range from 56-80% while Kellens et al. (2014) observed a SLS powder waste material rate of 45%. The high waste rates have been attributed to powder manufacturers' refresh rate recommendations and powder degradation over successive uses (Dotchev & Yusoff, 2009; Kellens et al., 2014; Telenko & Seepersad, 2010). Refresh rates are the ratios between virgin and recycled powder, as determined by powder manufacturers, to ensure acceptable part quality (Dotchev & Yusoff, 2009).

1.4.5. Comparisons with Other Additive Manufacturing Technologies

In their review of additive manufacturing environmental studies, Kellens, Baumers, et al. (2017) presented a schematic of SEC findings that indicates substantial variance among and within additive manufacturing processes. Of the plastic technologies, this review portrays stereolithography (SLA) and SLS as the most energy efficient with similar minimum and maximum values found in existing literature, while FDM reflected the highest reported SEC value. Considering the findings from Baumers et al. (2011), which were not included in the review by Kellens, Baumers, et al. (2017), SLS has a higher maximum SEC (237.68 MJ/kg) than SLA, but lower than FDM.

1.4.6. Comparisons with Conventional Manufacturing

Current life cycle assessment (LCA) literature indicates that conventional manufacturing generally has a lower environmental impact than additive manufacturing for industrial-scale production volumes, considering parts that could be produced with either process and achieve the requisite quality and functionality (Kellens, Mertens, et al., 2017). Specific energy consumption values for additive manufacturing unit processes have been reported as 1 to 2 orders of magnitude higher than conventional machining and injection molding processes (Gutowski et al., 2017; Kellens, Mertens, et al., 2017).

Few studies directly compare the energy consumption or environmental impact of SLS with injection molding. Telenko and Seepersad (2012) compared the cradle-to-gate energy consumption of SLS and injection molding for a plastic part, including the embodied energy of mold plate production and machining. Telenko and Seepersad (2012) found SLS was more energy efficient at lower volumes due to the significant energy consumption associated with mold production and machining, but that injection molding became the more energy efficient technology at higher volumes. The authors identified a breakeven production volume for SLS and injection molding between 50 to 300 parts for one design, and between 1,500 to 3,200 parts for another design, when injection molding became the more energy efficient process. The variance in crossover volumes depended on whether the mold was made of 100 percent virgin steel, steel with 80 percent recycled content, or aluminum with 20 percent recycled content. Telenko and Seepersad (2012) also highlighted the potential for a higher SLS and injection breakeven point if the part manufacturer used renewable electricity sources to power its machines instead of the grid, causing carbon emissions for SLS to become negligible.

Chen et al. (2015) arrived at a similar conclusion to Telenko and Seepersad (2012) in a case study comparing the embodied energy of SLS and injection molding across different batch sizes, finding that SLS had lower embodied energy for a batch size of 100 parts, but significantly higher embodied energy for batch sizes of 1,000 and 10,000 parts. Chen et al. (2015) highlighted that no economies of scale exist for SLS because the SEC of the process is constant, whereas the SEC for injection molding decreases as the production quantity increases.

2. Methods

This LCA utilizes process-based methods in accordance with the ISO 14040 standard to evaluate the cradle-to-gate life cycle primary energy consumption and GHG emissions of HP MJF additive manufacturing in relation to injection molding (International Organization for Standardization, 2006). Life cycle inventories are calculated for the raw materials, transportation, and manufacturing phases based on reference flows of 1 kilogram of mass using secondary data from several sources. Data for raw materials production and parameters for the MJF part manufacturing process originate from MJF technical documents and communications with HP representatives. Other sources for the LCIs in this report include: previous process LCAs and LCIs; ecoinvent 3.5; and Argonne National Laboratory's Greenhouse Gases, Regulation Emissions, and Energy Use in Transportation (GREET) 2019 model (Argonne National Laboratory, 2019a, 2019b; ATHENA Sustainable Materials Institute, 2002; Franklin Associates, 2011; Gutowski, Dahmus, & Thiriez, 2006; Wernet et al., 2016). Process parameters, inputs, and outputs are modeled using SimaPro 9.0.0.48 LCA software and Microsoft Excel spreadsheets.

2.1. Goals

The primary goal of this study is to improve decision-making in plastic part manufacturing by evaluating the primary energy consumption and GHG emissions of HP MJF 3D printing technology. Secondarily, this study seeks to understand the energy and environmental performance of MJF 3D printing as an alternative manufacturing process to injection molding across different volumes of production.

2.2. Scope

2.2.1. Life Cycle Phases

The scope of this life cycle assessment is cradle-to-gate, from raw materials extraction to completed manufacturing of the product. This study involves three cradle-to-gate LCAs of the product system with different manufacturing processes: (1) manufacturing with the HP MJF 4210 3D Printer and Processing station; (2) injection molding with aluminum tooling; and (3) injection molding with steel tooling.

2.2.2. MJF 3D Printing Process Flow and System Boundary

Figure 2 depicts the process flow and system boundary associated with the MJF 3D printing process. The product material inputs to the MJF process under investigation in this LCA are polyamide 12 (PA12, also referred to as Nylon-12), fusing agent, and detailing agent. Other ancillary material inputs that amortize over the production of multiple print jobs, such as the 3D printer's cleaning roll, maintenance kits, packaging, and part cleaning materials, are excluded from this study with the expectation that these inputs contribute less than 1% of the cradle-to-gate life cycle impact. Other product system components that amortize over their respective lifespans, such as the 3D printer, the processing station, and manufacturing facility infrastructure, are also excluded from this LCA. A screening analysis in **Section 2.6** supports the exclusion of MJF equipment. Maintenance of equipment, storage, and disposal of process waste also fall outside the scope of this LCA.

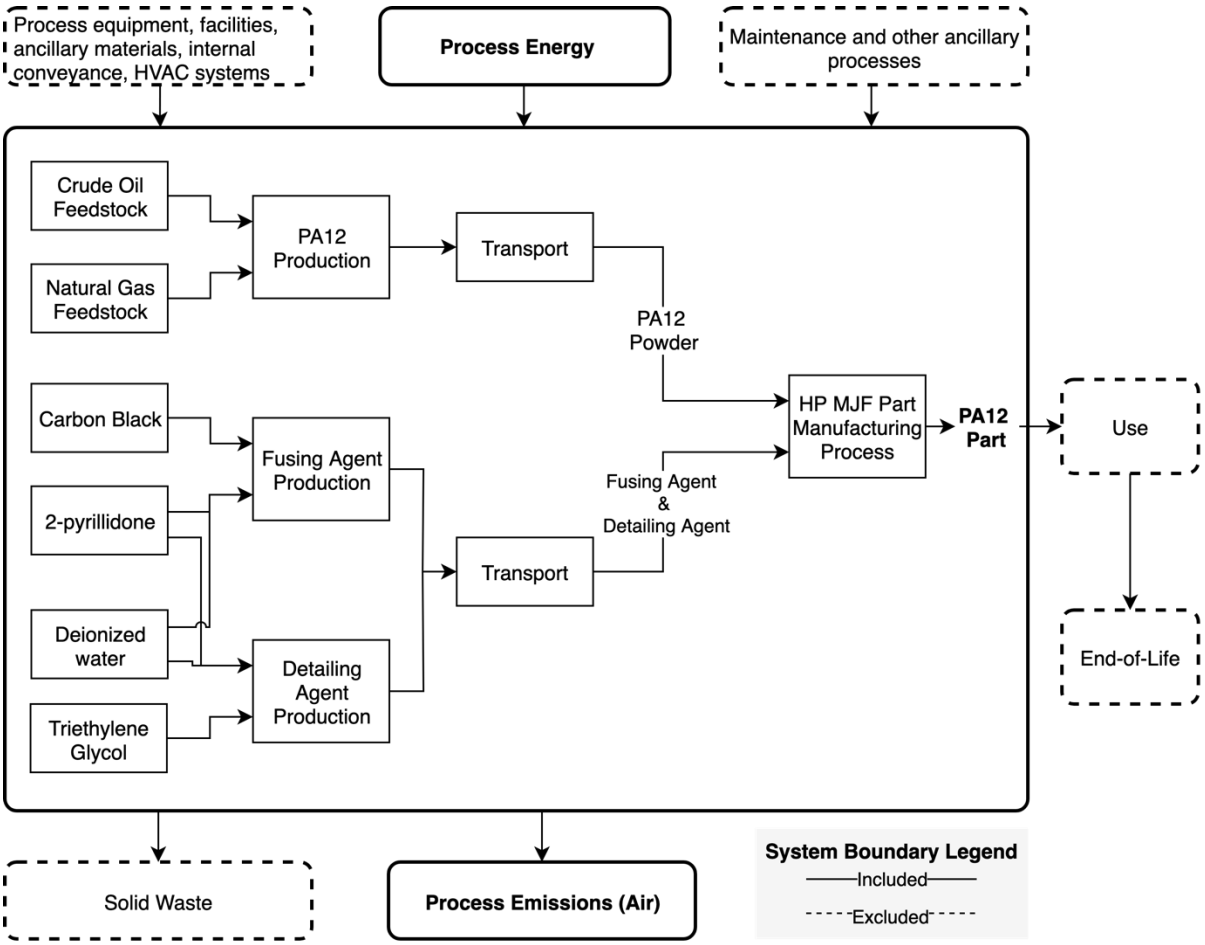

Figure 2. MJF Cradle-to-Gate Process Flow and System Boundary

Figure 3 shows the process flow within the MJF part manufacturing process. The part manufacturing process involves six primary steps: build platform file preparation, powder mixing and loading, MJF 3D printing, cooling, unpacking, and post-processing. This study evaluates LCI data across each of the steps except for the build file preparation step. The build file preparation step occurs primarily on desktop computers likely used for several other tasks and the contribution of the build file preparation step to the overall cradle-to-gate life cycle impact is assumed to be negligible.

Build file preparation. In this step, the user prepares the build platform computer-aided design (CAD) file, packing and orienting the parts appropriately within the build to optimize print speed and accuracy (HP Development Company L.P., 2019c).

Powder mixing and loading. After the user confirms the height of the build required for the print job, the user proceeds to the HP Jet Fusion 3D Processing Station, loads the built unit into the processing station, and inputs the required build height and the mix ratio of virgin powder and reclaimed powder (HP Development Company L.P., 2019c). The typical ratio recommend by HP is 80% reclaimed powder and 20% virgin powder (HP Development Company L.P., 2019c). The

processing station then loads the build unit with the required amount of powder according to the mix ratio.

MJF 3D Printing. Printing begins after loading of the build unit into the HP MJF 4210 3D printer and completion of printer set-up. Set-up takes approximately 1 hour and 30 minutes (D. Woodlock, personal communication, Jan. 3, 2020). The printing process proceeds as depicted in **Figure 1**, consuming fusing agent, detailing agent, and energy to fuse the powder into a solid object. The printing process takes approximately 10 hours with fast print mode or 16 hours and 20 minutes with the default/strength mode for a 100% full build chamber (HP Development Company L.P., 2019c). After completion of printing, the build unit remains in the printer for at least 30 minutes for safety cooling (HP Development Company L.P., 2019c).

Cooling. After the build finishes safety cooling in the printer, the user removes the build unit and chooses the cooling method: natural cooling or fast cooling. In the natural cooling method, the user sets the build unit aside until the temperature of the build chamber reaches 80°C (HP Development Company L.P., 2019c). For fast cooling, the user waits 3 to 4 hours, then inserts the build unit into the processing station, where the build chamber is chilled for approximately 10 hours in the case of a 100% full build (HP Development Company L.P., 2019c).

Unpacking. Once the build has cooled sufficiently, the parts are unpacked from the build unit using the vacuum in the processing station (HP Development Company L.P., 2019c). The vacuum collects the reusable powder material surrounding each part until the powder remaining on the part requires separate post-processing for removal (HP Development Company L.P., 2019c).

Post-processing. Post-processing for HP MJF parts after the unpacking step typically involves the use of abrasive blasting, such as sandblasting or glass bead blasting, in addition to air blasting (HP Development Company L.P., 2019c). Post-processing can be fulfilled by manual labor or use of automated equipment. This step is not supported by any HP 3D printing equipment. Post-processing techniques and equipment use are subject to the decisions of the part manufacturer, and this study evaluated the use of bead blasting.

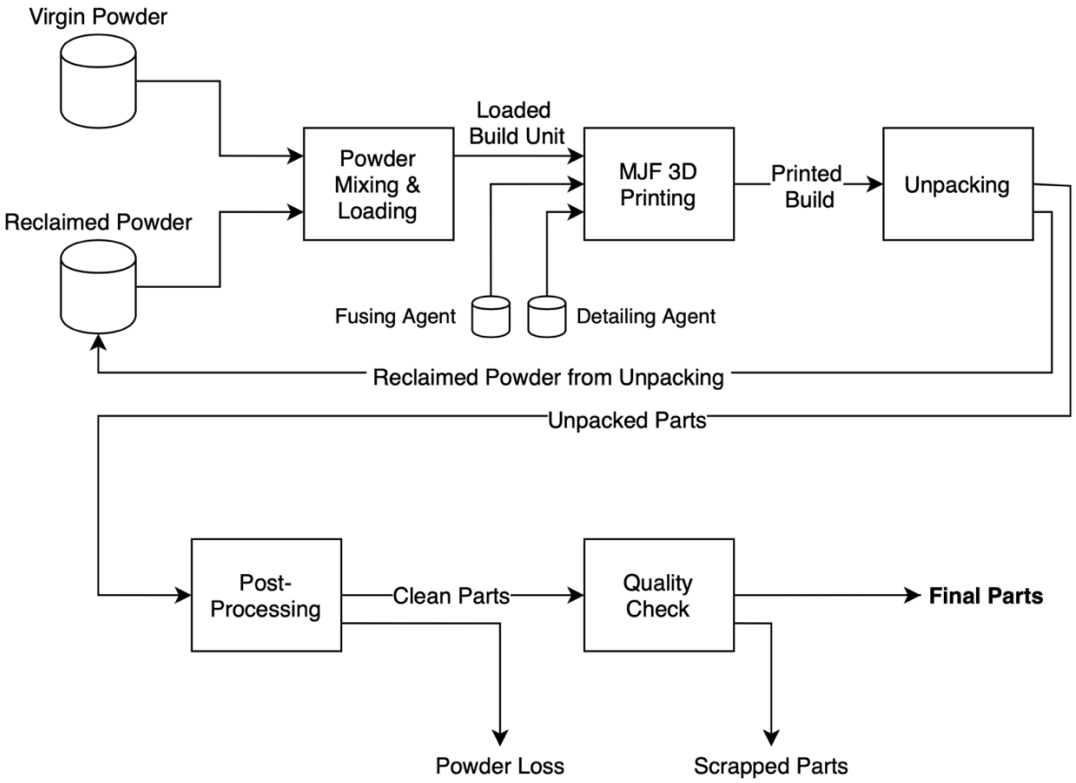

Figure 3. HP MJF Part Manufacturing Process Flow.

2.2.3. Injection Molding Process Flow and System Boundary

The injection molding process flow and system boundary are shown in **Figure 4**. The primary material inputs to the injection molding process are PA12 and the mold. The mold is included within the system boundary because it is created specifically for the functional unit. Two mold materials are assessed based on their prominence in injection molding: aluminum and steel. As with the MJF system boundary, ancillary materials and product systems that serve a general-purpose role for the injection molding process are excluded from the scope of the injection molding LCA.

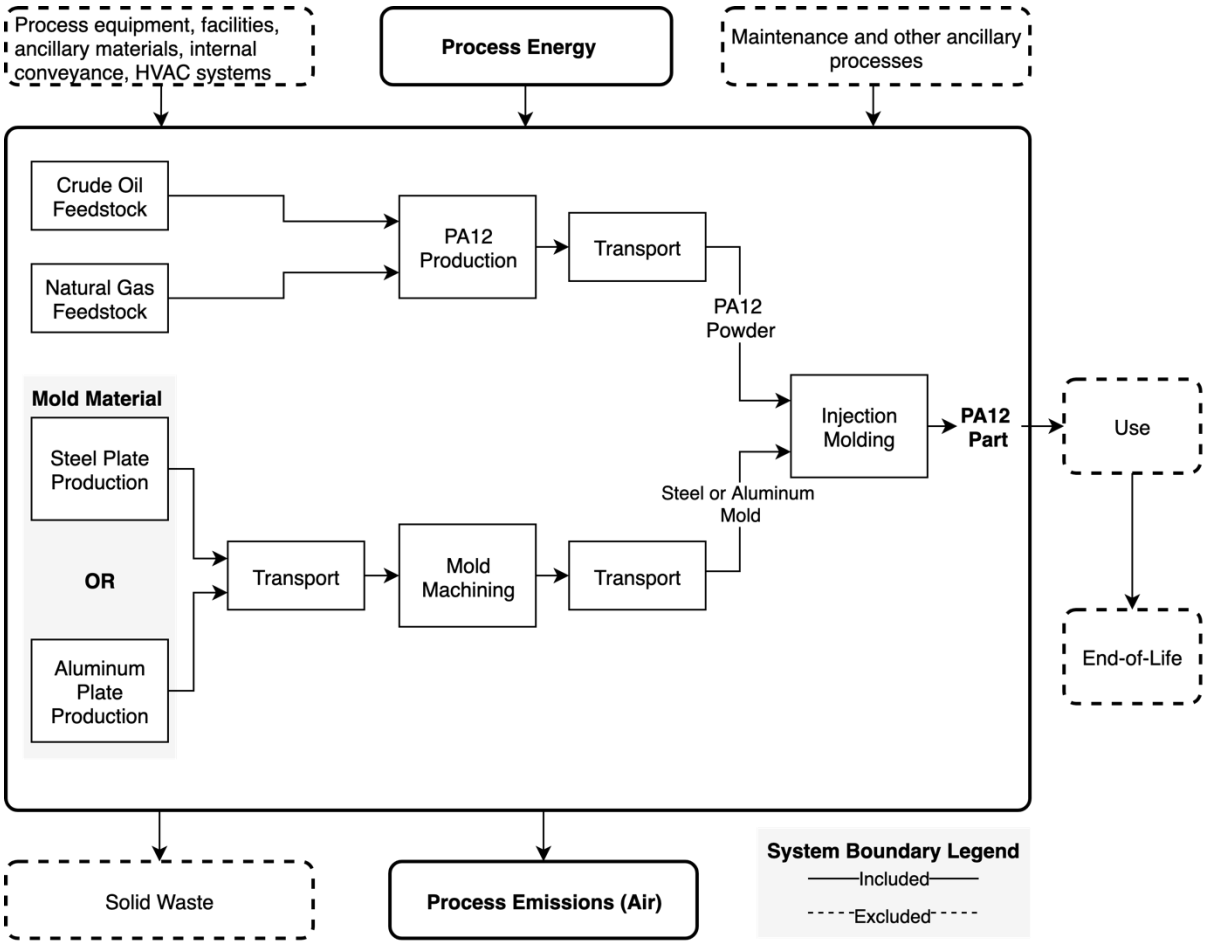

Figure 4. Injection Molding Process Flow and System Boundary.

2.2.4. Geography

This study models a manufacturing facility – Linear AMS – in Livonia, MI, as the destination for all input materials to the part manufacturing process. This manufacturing facility location is representative and appropriate for two reasons: (1) Michigan has the most establishments and highest employment in the industrial mold manufacturing industry; and (2) this company uniquely provides injection molding, mold machining, and MJF printing services under one roof ("Linear AMS," n.d.; U.S. Bureau of Labor Statistics, 2019). The production location of PA12 raw materials is Marl, Germany, which is the location of Evonik's PA12 production plants. Evonik is the dominant supplier of PA12 powder for additive manufacturing, including SLS and MJF, and also produces PA12 for injection molding (Evonik Resource Efficiency GmbH, n.d.-a, n.d.-b; Schmid, Kleijnen, Vetterli, & Wegener, 2017). Fusing agent and detailing agents were modeled with HP's 3D Open Platform Materials and Applications Lab in Corvallis, OR as the origin due to the lack of U.S. manufacturer location data (HP Development Company L.P., 2018b; HP Development Company L.P., 2020a). Rolling plants for steel and aluminum plates nearest to the Livonia manufacturing facility serve as the location for steel and aluminum plate production. ArcelorMittal's facility in Coatsville, PA – a P20 tool steel plate production plant – is the location for steel plate production (ArcelorMittal USA, 2015; American Metal Market, 2018). The Constellium Rolled Products Ravenswood aluminum plant in Ravenswood, WV serves as the location for aluminum plate production.

2.3. Functional Unit

The functional unit of the product system is the manufacturing of 100 LCD controller front covers made with PA12 (**Figure 5)**. This part serves as an appropriate functional unit because it is a typical plastic enclosure, and many industries require manufacturing of similar plastic enclosures, from automobiles to consumer electronics and medical devices (Sastri, 2010; Süli, 2019). Plastic enclosures can be manufactured across a variety of volumes depending on the particular application, and this part could be realistically considered for either 3D printing or injection molding depending on the application and quantity required. This study assumes the LCD controller front cover can be both injection-molded and additively manufactured with MJF technology based on the features of the part. The 3D computer-aided design (CAD) file for the LCD controller front cover originates from Thingiverse, a website that hosts user-submitted 3D models (Christou, 2013). **Table 1** lists key properties of the LCD controller front cover.

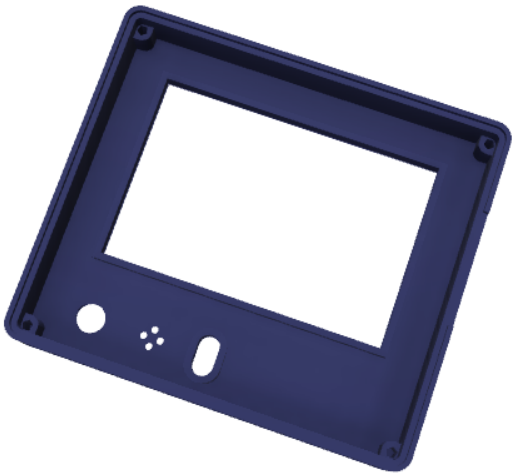

Figure 5. LCD Controller Front Cover

Table 1. LCD Controller Front Cover Properties

Property	**Value**
Surface Area	0.02693 m^2
Volume	30.02 cm^3
Product Mass	30.32 g
Bounding Box Length	108.6 mm
Bounding Box Width	95.4 mm
Bounding Box Height	16.1 mm

2.4. Life Cycle Assessment Metrics

This study measures cradle-to-gate life cycle energy consumption in units of megajoules [MJ] based on the primary energy of input material feedstocks, process fuels, process electricity consumption, and electricity grid generation mix. Cradle-to-gate life cycle GHG emissions are measured in units of kilograms of carbon dioxide equivalent [kg CO_2-eq] on a 100-year global warming potential time horizon using the values recommended by the Intergovernmental Panel on Climate Change Fifth Assessment Report (Myhre et al., 2013). The life cycle impact assessment considers these measures across production volumes ranging from 100 to 100,000 parts.

2.5. Fuel, Electricity Grid, and Emissions Data

This study uses 2020 time-series fuel, electricity grid, and emissions data from the GREET 2019 model to determine primary energy consumption and GHG emissions for the LCIs in this study, with the exception of PA12 production, and fusing and detailing agent production (Argonne National Laboratory, 2019a, 2019b). The PA12 production LCI uses data from EarthShift

Global, a consulting firm contracted by HP to conduct LCAs. LCIs for the fusing agent production and detailing agent production use ecoinvent 3.5 data with SimaPro 9.0.0.48 LCA software. Further detail on PA12 production and fusing and detailing agent production are provided in **Section 2.7.1** and **Section 2.7.2**, respectively.

The GREET 2019 model uses a 2015 North American Electric Reliability Corporation (NERC) region map to distinguish grid regions (Argonne National Laboratory, 2019a; North American Electric Reliability Corporation, 2015). Based on this region map, the RFC electricity grid generation mix applies to the part manufacturing facility, steel production facility, and aluminum production facility locations identified in **Section 2.2.4**.

2.6. Screening Analysis

A screening analysis on the potential cradle-to-gate life cycle impact of the MJF 3D printer, using data shown in **Table 2**, was conducted to determine whether to include production of MJF equipment in this study. Data for SLS 3D printing from Telenko and Seepersad (2012) were used to approximate the cradle-to-gate energy consumption of MJF for the additive manufacturing of one kilogram of PA12 product. The cradle-to-gate energy consumption data from Telenko and Seepersad (2012) account for the PA12 material embodied energy and the additive manufacturing site energy, excluding all other processes and materials. The results from Telenko and Seepersad (2012) for a full build chamber of parts indicate a cradle-to-gate energy consumption ratio of 327 MJ per kilogram of PA12 product.

Embodied energy data associated with the production of a selective laser melting (SLM) printer from Faludi, Baumers, Maskery, and Hague (2017) were used to approximate the embodied energy of an MJF 3D printer and scaled by weight. The same assumptions from Faludi et al. (2017) for service life, operating hours per day, operating days per week, and machine utilization were applied to determine the total operating hours of the MJF 3D printer over its 8 year service life. Two weeks out of the year were allocated for holidays and a maintenance period. The approximate time for an MJF 3D printing job was sourced from the HP Jet Fusion 4200 3D Printing Solution User Guide, assuming a 100% full build chamber on fast printing mode at 10% packing density with an additional 1.5 hours for setup time. The resulting ratio of machine embodied energy per kilogram of product was 3.67 MJ/kg.

The machine embodied energy ratio divided by the cradle-to-gate energy consumption ratio for one kilogram of PA12 product is 1.12%. This result suggests that the 3D printer accounts for approximately 1.12% of the cradle-to-gate life cycle impact for an additively manufactured PA12 product. However, this proportion reflects site energy consumption for the additive manufacturing process rather than primary energy consumption. The contribution of the 3D printer to the cradle-to-gate life cycle impact of a PA12 product is likely lower than 1.12% due to upstream energy generation, transmission, and distribution inefficiencies. The MJF processing station is expected to have less impact per kilogram of PA12 product than the MJF 3D printer due to the processing station's smaller mass and reduced complexity associated with internal components (sieve, powder mixer, vacuum). Consequently, both the MJF 3D printer and processing station were excluded from the system boundary.

Table 2. MJF 3D Printer Embodied Energy Estimation

Parameter	**Value**	**Unit**
Renishaw AM250 SLM printer mass[a]	1,215	kg
Renishaw AM250 embodied energy	124,000	MJ
Renishaw AM250 energy:mass ratio	102	MJ/kg
MJF 3D 4210 Printer mass[b]	750	kg
Estimated MJF 3D 4210 embodied energy	76,543	MJ
MJF 3D 4210 printer estimated service life[c]	8	years
Operating hours per day[c]	24	hr
Operating days per week[c]	7	days
Operating weeks per year[d]	50	weeks
Machine utilization[c]	90	%
Operating hours over service life	60,480	hr
Approximate printing time per job[e]	12.00	hr
Number of print jobs over service life	5040	print jobs
Material mass produced per print job at 10% packing density[f]	4.14	kg
Total material mass printed over service life	20,876	kg
MJF 3D 4210 embodied energy per kg material produced	3.67	MJ/kg
SLS cradle-to-gate primary energy consumption benchmark[g]	327	MJ/kg
Estimated MJF 3D 4210 printer cradle-to-gate LCA contribution	1.12	%

*Note***.** Screening analysis data to estimate the contribution of the MJF 3D printer and processing station to the overall cradle-to-gate life cycle impact for an additively manufactured PA12 part.

[a] Sourced from Faludi, Baumers, Maskery, and Hague (2017)

[b] Sourced from HP Jet Fusion 3D 4210 data sheet

[c] Service life, operating hours and days, and utilization assumptions based on Faludi, Baumers, Maskery, and Hague (2017)

[d] Assumed two weeks off for holidays and maintenance period.

[e] Sourced from HP Jet Fusion 4200 3D Printing Solution User Guide, assuming a 100% full build chamber on fast printing mode at 10% packing density. Applied additional 1.5 hours applied for setup time based on communication with HP (D. Woodlock, personal communication, Jan. 3, 2020).

[f] Calculated based on PA12 density of 1.01 g/cm^3.

[g] Adapted from Telenko and Seepersad (2012)

2.7. Multi-Jet Fusion Life Cycle Inventory

2.7.1. Raw Materials – PA12

The MJF and injection molding processes use different forms of the same PA12 material as manufacturing inputs. MJF uses PA12 powder while injection molding uses PA12 pellets. In both cases, peer-reviewed life cycle inventory data for PA12 are not publicly available. For this reason, previous LCAs on additive manufacturing with SLS used LCI data for polyamide 6 (PA6) as modeling inputs for raw materials (Telenko & Seepersad, 2010, 2012; Kellens et al., 2014). In this case, the polymer's associated PlasticsEurope Eco-profile states that the cradle-to-gate primary energy and GHG emissions for production of 1 kg of PA6 are 129.1 MJ and 6.7 kg CO_2-eq, respectively (PlasticsEurope, 2014).

Despite the use of PA6 LCI data as a substitute for PA12 in prior literature, two sources of unpublished data provide a different basis for this study's raw material modeling assumptions. An eco-profile report by Arkema, one of the main manufacturers of PA12, compares polyamide 11 (PA11) to other polymers, including PA12. In this report, Arkema notes that the gross energy requirement for PA12 is 207 MJ/kg and the GHG emissions are 6.9 kg CO_2-eq (Devaux, Lê, & Pees, n.d.). Separately, communications with EarthShift Global provided cradle-to-gate cumulative energy demand and emissions data for production of 1 kg of PA12 resin: 345 MJ and 15.39 kg CO_2-eq (L. Laurin, personal communication, Jan. 24, 2020, Feb. 7, 2020). HP and EarthShift Global could not release additional information on the production of PA12 due to non-disclosure agreements. Neither source of PA12 LCI data provide information regarding the difference, if any, in energy consumption required for transformation into powder or pellet forms. As a conservative approach, this study uses the EarthShift Global data for modeling. This study assumes the cumulative energy demand is the same for production of PA12 powder and pellet forms due to the lack of available data. Sensitivity analyses in Section 3.4.3 explore the potential variance in LCA results when using PA6 data.

2.7.2. Raw Materials – Fusing and Detailing Agents

Material Safety Data Sheets (MSDS) for HP's MJF fusing and detailing Agents provide information on their chemical composition that can be used to support LCI data calculations. The main ingredients for the fusing agent are water, 2-pyrrolidone, and a black pigment with an unspecified amount of carbon black (HP Development Company L.P., 2020b). For the detailing agent, the main ingredients are water, 2-pyrrolidone, and triethylene glycol (HP Development Company L.P., 2020c). The associated patent refers to these agents as ink-type formulations (Patent No. 10,392,512 B2, 2019); therefore, this study modeled the manufacturing of the agents based on printing ink production LCI data from the ecoinvent 3.5 database in SimaPro. According to Krystofik, Babbitt, & Gaustad (2014), comparable ink formulations to an HP 60 inkjet cartridge primarily use deionized water. This study made assumptions shown in **Table 3** regarding the percentage for each ingredient, which were conservatively chosen near the upper bounds of the percentages identified in the respective MSDS.

Table 3. Fusing and Detailing Agent Production LCI (for 1kg of product)

Inputs	Qty		Unit
	Fusing Agent	**Detailing Agent**	
Materials			
2-pyrrolidone[a]	0.19	0.04	kg
Carbon black[b]	0.07	-	kg
Triethylene glycol[c]	-	0.14	kg
Deionized water[c]	0.74	0.82	kg
Energy			
2-pyrrolidone production[a]	30.97	6.52	MJ
Carbon black production[b]	5.37	-	MJ
Triethylene glycol production[c]	-	6.02	MJ
Deionized water production[d]	0.01	0.01	MJ
Electricity, agent manufacturing[e]	4.21	4.21	MJ
Natural gas, agent manufacturing[e]	3.68	3.68	MJ
Total primary energy	44.24	20.44	MJ
Emissions			
GHG emissions	2.22	1.06	kg CO_2-eq

Note. Assumptions are based on HP fusing agent and detailing agent MSDS. Energy values are calculated using SimaPro software with ecoinvent 3.5 database and Cumulative Energy Demand V1.00/Cumulative energy demand/Single Score impact method (Wernet et al., 2016). Emissions values are calculated using IPCC 2013 GWP 100a V1.03/Characterization method for 2-pyrrolidone, carbon black, triethylene glycol, and deionized water, and GREET2 2019 model for calculation of GHG emissions for electricity and natural gas (Argonne National Laboratory, 2019b).

[a] 2-pyrrolidone {GLO}|market for | APOS, U; percent composition of fusing agent - 19%; percent composition of detailing agent: 4%.

[b] Carbon black {GLO}|market for|APOS,U; percent composition of fusing agent - 7%

[c] Triethylene glycol {RER} | market for triethylene glycol|APOS, U; percent composition of detailing agent - 14%.

[d] Water, deionised, from tap water, at user {Europe without Switzerland}|market for water, deionised, from tap water, at user|APOS,U; percent composition of fusing agent - 74%; percent composition of detailing agent: 82%.

[e] Based on ecoinvent 3.5 data for: 1 kg printing ink, offset without solvent, in 47.5% solution state {RER}| printing ink production, offset, product in 47.5% solution state |APOS, U (Wernet et al., 2016). Assumed all on-site heat energy derived from natural gas combustion.

2.7.3. Transportation – PA12

This study used the Distance & Time Tool on Searates.com to calculate the trucking and ocean freight distance required to transport PA12 from the raw materials processing facility in Marl, Germany to the part manufacturing facility in Livonia, MI : 44 miles by truck and 3,801miles by ocean freight ("Distances & Time," n.d.). Searates.com identified Duisburg as the departure port in Germany and Detroit City as the arrival port in Michigan.

LCI data for trucking and ocean freight transportation shown in **Table 4** originate from the GREET1 2019 Heavy-Duty Vehicles (HDV) Well-to-Wheel (WTW) and Marine Well-to-Hull (WTH) modules. This study assumed light heavy-duty vocational vehicles powered by compression-ignition, direct-injection (CIDI) diesel engines from the HDV WTW module as the

vehicle type for PA12 transportation. In the Marine WTH module, bulk, foreign vessels transported the PA12 materials across the Atlantic Ocean.

Table 4. Trucking & Ocean Freight Transportation Mode LCI (for 1 tonne-mi)

Inputs	**Qty**	**Unit**
Trucking energy[1]	6.41	MJ
Ocean freight energy[2]	0.147	MJ
Emissions		
Trucking emissions[1]	0.492	kg CO_2-eq
Ocean freight emissions[2]	0.011	kg CO_2-eq

Note. Data are calculated with GREET1 2019 model (Argonne National Laboratory, 2019a).
[a] HDV WTW for Light Heavy-Duty Vocational Vehicle and CIDI Vehicle: Diesel - 2020 simulation
[b] Marine WTH for Bulk, Foreign, Atlantic (Cruise distance: 3801.43 nm) - 2020 simulation

2.7.4. Transportation – Fusing and Detailing Agents

According to Google Maps, the trucking distance required to transport the fusing and detailing agents 12 from the facility in Corvallis, Oregon to the part manufacturing facility in Livonia, Michigan is 2,382 miles.

2.7.5. Part Manufacturing – HP Multi-Jet Fusion 3D Printing

This LCA evaluates electricity consumption of the part manufacturing phase for the MJF process and the associated GHG emissions; data for direct emissions from MJF equipment are not available, but are assumed negligible for modeling purposes.

Build Platform File Preparation. This study used Autodesk Netfabb 2019 to design the build platform file, packing parts into the platform with the software's automated 3D Packing – Monte Carlo tool. This tool is useful for packing a large number of parts and minimizing the packed platform height (Autodesk Inc., 2020a, 2020b). Assuming a scrap rate of 5% for the MJF process, 106 parts are required to produce the 100-part functional unit. Although communication with HP suggested a scrap rate of 1.5%, this study uses 5% to be more conservative (D. Woodlock, personal communication, Apr. 13, 2020).

Table 5 depicts the build platform setting results from the 3D Packing – Monte Carlo tool for the 106 LCD Controller Front Cover and **Figure 6** shows an image of the associated packed build platform. The maximum number of parts that could be packed on the build platform with the 3D Packing – Monte Carlo tool is 108 (see **Table 5** for the associated build platform settings). This study modeled part production quantities greater than 100 by first determining the number of maximum builds necessary that could be completed and allocating the remaining parts to a partial build.

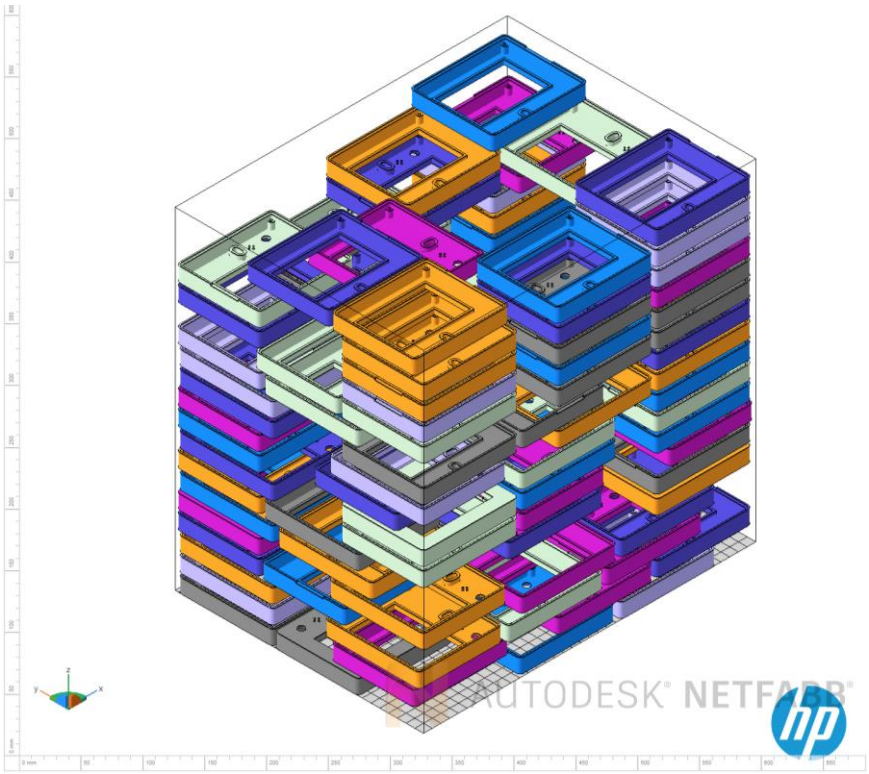

Figure 6. Packed Build Platform for 100 Final Parts.

Table 5. Build Platform Settings for Functional Unit Build and Maximum Part Build

Setting	Value	
	Functional Unit Build	**Maximum Part Build**
Number of parts packed in build platform	106	108
Build height (mm)	365.14	365.14
Packing density	8.075%	8.227%

Note. Packed with Autodesk Netfabb 3D Packing - Monte Carlo function; min. distance between parts - 2.0 mm; all other settings – default. Assumed 5% scrap rate; 106 printed parts required to obtain 100 final parts.

Table 6 shows the number of maximum parts builds, partial builds, and associated partial build platform settings for selected part production quantities from 250 to 100,000 parts. The build platform settings from **Table 5** and **Table 6** feed directly into the model for calculating the energy consumption associated with the next four steps.

Table 6. Build Data for Production Volumes from 250 to 100,000

Desired number of parts	**250**	**500**	**1,000**	**2,500**	**5,000**
Required number of printed parts	264	527	1,053	2,632	5,264
Number of maximum parts builds	2	4	9	24	48
Remaining number of parts for partial builds	48	95	81	40	80
Partial build - build height	159.8	324	283	139.3	283
Partial build - packing density	8.35%	8.15%	7.96%	7.99%	7.86%
Desired number of parts	**10,000**	**25,000**	**50,000**	**100,000**	
Required number of printed parts	10,527	26,316	52,632	105,264	
Number of maximum parts builds	97	243	487	974	
Remaining number of parts for partial builds	51	72	36	72	
Partial build - build height	180.4	242	118.8	242	
Partial build - packing density	7.87%	8.28%	8.43%	8.28%	

Powder Mixing and Loading. In this step, the HP MJF 4210 Processing Station consumes electricity to mix and load PA12 powder in the build unit.

Table 7 shows the characteristics of the HP MJF 4210 Processing Station associated with the powder and mixing step, sourced from HP MJF technical documents and communications with HP employees (HP Development Company L.P., 2019b, 2019c; H.T. Etheridge, personal communication, Jan. 28, 2020).

Table 7 also identifies modeling assumptions made regarding power consumption during idle state, setup, powder mixing, and powder loading due to the lack of available data for these characteristics. This study further assumed a linear increase in time for powder mixing and loading between the times listed in the HP Jet Fusion 4200 User Guide to facilitate the calculation of process time for all build heights in the absence of additional data from HP.

Table 7. HP MJF 4210 Processing Station Characteristics – Powder Loading & Mixing

Characteristic	**Data**	**Unit**
Setup time[a]	0.167	hr
Idle/setup/natural cooling power consumption[b]	0.3	kW
Powder mixing & loading power consumption[c]	2.6	kW
Powder mixing & loading time, 80% recycled & 20% fresh material[d]		
100% full chamber	1.250	hr
75% full	0.958	hr
50% full	0.625	hr
25% full	0.333	hr

Note. Data are adapted from HP MJF 4210 datasheet and HP Jet Fusion 4200 User Guide (HP Development Company L.P., 2019b, 2019c).

[a] Assumed 10 minutes based on setup procedures in HP Jet Fusion 4200 User Guide for powder loading/mixing.

[b] Assumed to be same as idle power for HP MJF 4210 3D printer

[c] Sourced from HP MJF 3D 4210 Solution data sheet; assumed constant throughout powder mixing and loading.

[d] Applied median mixing and loading times from HP Jet Fusion 4200 User Guide, p. 73

MJF 3D Printing. Although energy intensity is expected to vary over the duration of a print job based on packing density, printing speed, and other factors, the energy profile of the MJF 3D printer was not available from public sources or HP. This study models the power consumption for the MJF 3D printer using a constant 0.3 kW for idle status and constant 8.525 kW for printing based on communications with the HP LCA Program Manager (H.T. Etheridge, personal communication, Jan. 28, 2020). This contrasts slightly with the HP MJF 4210 datasheet, which indicates a typical power consumption for the 3D printer of 9-11 kW; however, the data from the HP LCA Program Manager are assumed to be more accurate (HP Development Company L.P., 2019b). Printer setup and safety cooling are assumed to require the same amount of power as printer idling. **Table 8** list the characteristics of the MJF 3D printer used for energy consumption modeling.

Energy consumption for the print job is calculated based on idle time, idle power, build volume, printing speed, and printing power using Equation 1:

$$\textbf{(1)}\ \boldsymbol{E_{MJF\_PRINT} = (t_{IDLE} \times P_{IDLE})\left(\left(\frac{V_{BUILD}}{S_{PRINT}}\right) \times P_{PRINT}\right)}$$

where $E_{MJF_PRINT}$is the energy consumption of the print job; t_{IDLE} is the time the printer spends in idle status, setup, and safety cooling; P_{IDLE} is the idle power consumption during idle status, setup, and safety cooling; V_{BUILD} is the volume of the build; S_{PRINT} is the printing speed; and P_{PRINT} is the 3D printer's power consumption during printing. Considering energy consumption increases based on the duration of printing time, this model applied the fast printing speed to understand the minimum amount of energy required for the MJF process. This model assumes the power consumption is the same for both printing speeds in the absence of additional data from HP.

Table 8. HP MJF 4210 3D Printer Characteristics

Characteristic	**Data**	**Unit**
Build chamber (L x W x H)	380 x 284 x 380	mm
Build chamber volume[a]	41,010	cm^3
Default/strength printing speed[b]	2,519	cm^3/hr
Fast printing speed	4,115	cm^3/hr
Idle power consumption[c] (including setup & safety cooling)	0.3	kW
Printing power consumption[d]	8.525	kW
Setup time[e]	1.5	hr
Safety cooling time	.5	hr

Note. Data are adapted from HP MJF 4210 datasheet and HP Jet Fusion 4200 User Guide (HP Development Company L.P., 2019b, 2019c).

[a] Calculated based on build chamber dimensions.

[b] Calculated based on HP Jet Fusion 4200 User Guide default/strength mode printing time for full chamber build.

[c] Provided by HP LCA Program Manager.

[d] HP MJF 4210 datasheet states 9-11 kW for average power consumption. However, the HP LCA Program Manager identified actual print power as 8.525 kW.
[e] Provided by HP MJF Market Development Manager.

Cooling and Unpacking. **Table 9** shows the electricity consumption data used for modeling of cooling and unpacking. Due to the lack of power profile data for the processing station, electricity consumption data for cooling and unpacking were assumed to be the same as powder loading and mixing. Power consumption is also assumed to be constant throughout fast cooling and unpacking. Similarly, setup time for both cooling and unpacking were assumed to be 10 minutes based on the procedures in the HP Jet Fusion 4200 User Guide.

Table 9. HP MJF 4210 Processing Station Characteristics – Cooling and Unpacking

Characteristic	**Data**	**Unit**
Setup time	0.167	hr
Idle/setup/natural cooling power consumption[2]	0.3	kW
Fast cooling power consumption/Unpacking power consumption[3]	2.6	kW

*Note***.** Data are adapted from HP Jet Fusion 4200 User Guide and HP MJF 4210 datasheet.

Post-processing. Although most additively manufactured parts require some form of post-processing, no LCI data exist on these processes. The impacts of post-processing have mostly been neglected or underestimated in previous environmental studies of additive manufacturing (Kellens, Baumers, et al., 2017; Kellens, Mertens, et al., 2017). Despite this research need, development of empirically supported LCI data for post-processing of MJF parts requires substantial research outside the scope of this study due to the wide variance of potential surface finishing requirements and post-processing methods. Consequently, this study performed screening-level research to provide an approximate understanding of the relative contribution from this step to the overall cradle-to-gate energy and environmental impacts of the HP MJF process.

A case study by PostProcess Technologies Inc. indicates that a small part with a similar bounding box dimensions to the LCD Controller Front Cover requires 1 minute of manual air/bead blasting time per part (PostProcess Technologies Inc., n.d.). Suggestions for air pressure range from 2-5 bar for bead blasting and 4 bar for air blasting non-fragile parts (HP Development Company L.P., 2017b, 2018a). This study assumed 4 bar (58 psi) and 1 minute to complete bead blasting for each part due to the LCD controller front cover's relatively small size and low complexity. According to Clemco Industries Corp., a 1/4" nozzle orifice with 60 psi at the nozzle requires 54 cubic feet per minute and a compressor rated at a minimum of 12 hp (Clemco Industries Corp, 2007). This study assumed a 90% motor efficiency based on the average threshold efficiency values for 15 hp general purpose motors manufactured for sale in the U.S. (U.S. Department of Energy, 2014). This study used a formula from U.S. Department of Energy (2003) for calculating the cost of compressed air to determine bead blasting electricity consumption, shown in Equation 2, as 0.166 kWh per LCD controller front cover.

$$(2)\ \boldsymbol{Electricity\ (kWh)} = \frac{(\boldsymbol{Compressor\ hp})\times(\mathbf{0.746}\frac{\boldsymbol{kW}}{\boldsymbol{hp}})\times(\boldsymbol{Air/Bead\ Blasting\ hr})}{\boldsymbol{Motor\ efficiency}}$$

The powder removed from each part during post-processing is typically unusable and amounts to approximately 10% of the part mass (HP MJF 3D Printing Market Development Manager, personal communication, Jan. 3, 2020). Telenko and Seepersad (2010) also report a 10% excess powder loss in the equivalent step of the SLS process.

2.8. Injection Molding Life Cycle Inventory

2.8.1. Raw Materials – Plastic Injection Molds

This study uses the two-plate mold structure for modeling of mold raw materials and machining because it is the most commonly used mold design for plastic injection molding (Campo, 2006). Boothroyd, Dewhurst, and Knight (2010) provide design rules to estimate the combined cavity and core plate thickness based on a part's dimensions, the number of cavities, and the cavity layout. Assuming a single-cavity mold, **Table 10** depicts the minimum plate dimensions for the LCD controller cover.

Table 10. Cavity and Core Plate Dimensions

Dimension	**Value (cm)**
Plate Length	25.86
Plate Width	24.54
Combined Cavity & Core Plate Thickness	16.61

To determine the material mass of the mold, a computer-aided design (CAD) file for a standard two-plate mold was downloaded from the mold base catalog of the DME Company, a major mold component supplier (DME Company, 2020). Using the dimensions in **Table 10**, the most suitable mold base design in the DME catalog is XPress™ A-Series Mold Base Model 1012 shown in
Figure 7. **Table 11** lists the material volume of the major components in this mold base.

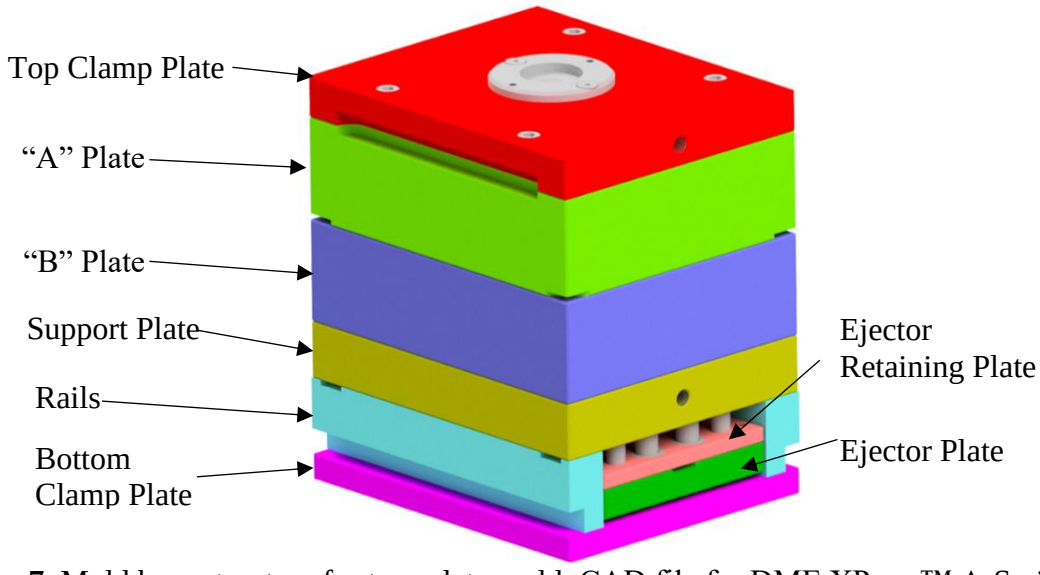

Figure 7. Mold base structure for two-plate mold. CAD file for DME XPress™ A-Series Mold Base Model 1012 from DME Company Configurator site (DME Company, 2020). Rendered image using Autodesk Inventor 2019.

Table 11. Mold Base Component Volumes

Component	Volume (cm^3)
Top clamp plate	2,418.58
"A" plate	6,227.38
"B" plate	6,124.70
Support plate	3,423.22
Rails (both)	1,132.61
Ejector retaining plate	615.12
Ejector plate	1,249.24
Bottom clamp plate	1,607.52
Total	22,798.37

In *Injection Mold Design Engineering*, Kazmer (2016) provides equations to estimate the dimensions of the core and cavity inserts. Using Kazmer's (2016) equations 3.16 and 3.17, **Table 12** below depicts the estimated dimensions of the cavity set.

Table 12. Cavity Set Dimensions

Component	Value	Unit
Length	24.54	cm
Width	25.86	cm
Height	16.61	cm
Volume	10,540.78	cm^3

Plastic injection molds can be fabricated and assembled from various materials, including both ferrous and non-ferrous metals (Geng, 2016; Kazmer, 2016). A common injection molding strategy for production volumes between 500 and 200,000 parts involves the use of aluminum tooling (Kazmer, 2016). Mold bases made from aluminum commonly use 7075-T6 grade aluminum (Kazmer, 2016b). For higher production volumes, the majority of plastic injection molds are made of AISI P20 grade tool steel (Kazmer, 2016; Mesquita, 2016). Given the volume for each mold base component and the cavity set, **Table 13** lists the mass values for the aluminum mold based on a density of 2.81 g/cm^3 for 7075-T6 aluminum and the steel mold based on a density 7.850 g/cm^3 for AISI P20 tool steel.

Table 13. Mold Component Mass

Component	Mass (kg)	
	Aluminum	Steel
Top clamp plate	6.80	18.99
"A" plate	17.50	48.88
"B" plate	17.21	47.08
Support plate	9.62	26.87
Rails (both)	3.18	8.89
Ejector retaining plate	1.73	4.83
Ejector plate	3.51	9.81
Bottom clamp plate	4.52	12.62
Cavity set	29.62	82.75
Total	93.68	261.71

2.8.1.1. Aluminum Molds

LCI data are not publicly available for 7075 grade aluminum. For this reason, this study uses LCI data from GREET2 2019 for flat-rolled virgin wrought aluminum and recycled wrought aluminum, assuming a metal composition of 67.5% recycled aluminum (The Aluminum Association, 2013). **Table 14** depicts the LCI data for the aluminum tooling used in this study.

Table 14. Aluminum Plate LCI (for 1 kg of Al plate)

Inputs	**Qty**	**Unit**
Total energy for flat-rolled virgin aluminum share	43.8	MJ
Total energy for flat-rolled recycled aluminum share	16.0	MJ
Total primary energy	59.8	MJ
Emissions	**Qty**	**Unit**
GHG emissions for flat-rolled virgin aluminum share	2.7	kg CO_2-eq
GHG emissions for flat-rolled recycled aluminum share	1.0	kg CO_2-eq
Total GHG emissions	3.7	kg CO_2-eq

Note. Wrought aluminum data are from GREET2 2019; calculated with GREET2 2019 RFC electric grid mix - 2020 simulation (Argonne National Laboratory, 2019b).

[a] Assumes aluminum plate metal composition as 32.5% flat-rolled virgin aluminum and 67.5% recycled aluminum.

2.8.1.2. Steel Molds

Energy consumption and GHG emissions life cycle inventory data is not publicly available for the specific grades of steel plates used in the DME XPress™ A-Series Mold Base. A potential source of data for P20 tool steel is a paper by Minetola and Eyers (2018). In their comparison of injection molded and 3D printed mobile case covers, Minetola and Eyers (2018) cite life cycle energy consumption data for P20 tool steel from Cambridge Engineering Selector (CES) EduPack Software by Granta Design Limited (2016): 25.65 MJ for P20 steel production embodied energy and 11.50 MJ for P20 steel casting energy. However, the authors do not provide greenhouse gas emissions data associated with P20 steel production and casting.

Considering the lack of publicly available LCI data, this study calculated LCI data for steel plates assuming the use of the electric arc furnace (EAF) steel production. The EAF route is the primary process for manufacturing tool steels (Mesquita, 2016). Moreover, 67.3% of crude steel production in the U.S. uses the EAF process (World Steel Association, 2019). The EAF route typically consists of melting, ladle furnace refining, vacuum degassing, and casting (Mandal, 2015; Mesquita, 2016). After casting, the steel slabs proceed to hot rolling at a plate mill (Mandal, 2015). This study used the ATHENA Sustainable Materials Institute's (2002) *Cradle-To-Gate Life Cycle Inventory: Canadian and U.S. Steel Production by Mill Type* to calculate LCI data for the steel plates shown in **Table 15**.

Table 15. Steel Plate LCI (for 1kg of steel plate)

Inputs	**Qty**	**Unit**
Materials		
Scrap metal	0.79	kg
Direct reduced iron	0.70	kg
Lime/refractories/electrodes	0.09	kg
Energy		
Electricity		
Mining & Pelletizing Ore	3.34	MJ
MIDREX	1.65	MJ
EAF - Flat Rolled Products	13.77	MJ
LMF	0.38	MJ
Slab caster	0.53	MJ
Plate Mill	2.18	MJ
Natural Gas		
Mining & Pelletizing Ore	0.05	MJ
MIDREX	9.25	MJ
EAF - Flat Rolled Products	0.33	MJ
Slab caster	1.40	MJ
Plate Mill	3.63	MJ
Fuel oil		
Mining & Pelletizing Ore	0.40	MJ
Diesel		
Mining & Pelletizing Ore	0.07	MJ
Rail Transportation - Pellets	0.19	MJ
Total primary energy	37.18	MJ
Emissions		
GHG emissions	2.49	kg CO_2-eq

Note. LCI data are adapted from ATHENA Sustainable Materials Institute (2002). Primary energy and emissions are calculated with GREET2 2019 RFC electric grid mix - 2020 simulation.

2.8.2. Transportation – Mold Plates

Distribution centers and warehouses between the plate production sites and part manufacturing facility were omitted to represent the minimum distance requirement for transportation of the mold plates. Trucking distances were calculated using Google Maps: 545 miles for steel plates transportation and 324 miles for aluminum plates.

2.8.3. Part Manufacturing – Mold Machining

LCI data for mold machining vary significantly across publicly available literature. This variance occurs because the time and energy consumed during mold machining depends on several variables, including the machining tools and processes used, volume and geometric complexity of the part to be molded, mold material properties, and the surface quality requirements of the mold (Kazmer, 2016a). For example, Ribeiro, Peças, and Henriques (2008) used three different processes for mold machining in their life cycle assessment of plastic injection mold production: milling, drilling, and electric discharge machining (EDM). Within the milling process alone, Yoon et al. (2014) reported specific energy consumption values ranging from 6.8 to 188 J/mm^3 from prior studies for cutting with different types of steel. Moreover, the milling process is often separated into rough and finish milling – also referred to as coarse and fine machining – that involve different processes to remove large amounts of material and more detailed operations to ensure dimensions and surface quality fall within required tolerances (Morrow et al., 2007; Minetola & Eyers, 2018). Morrow et al. (2007) reported 24 MJ/kg for rough machining and 600 MJ/kg for fine machining of an H13 tool steel mold, while Minetola and Eyers (2018) cited 1.78 MJ/kg for coarse machining, 13.35 MJ/kg for fine machining, and 26.20 MJ/kg for grinding of P20 steel mold based on LCI data from Granta Design Limited Cambridge Engineering Selector (CES) EduPack software. Finally, the total energy consumption of machine tool use depends on the time and power requirements across three stages of operation: start-up, run-time, and cutting (Dahmus & Gutowski, 2004).

Considering the wide variance of machining LCI data and the primary focus of this study on the MJF process, a simplified approached to estimate energy consumption and GHG emissions is used here. Based on the mold cost estimation framework in *Injection Mold Design Engineering*, this study assumes the approximate volume of the mold material to be removed by machining is equal to the entire volume of the cavity set (Kazmer, 2016a). This volume is applied to material removal electricity consumption data from Dahmus and Gutowski (2004) and to the U.S. RFC grid to ascertain the total primary energy and greenhouse gas emissions shown in **Table 16**.

Table 16. Mold Machining LCI (for 1 cm3 material removed)

	Quantity		
Inputs	**Aluminum**	**Steel**	**Unit**
Primary energy	0.0316	0.1343	MJ
Emissions			
GHG emissions	0.0022	0.0093	kg CO_2-eq

Note. LCI data are based on production machining center electrical energy consumption for aluminum and steel from Dahmus and Gutowski (2004). Determined primary energy and GHG emissions with GREET1 2019 data for RFC grid, 2020 time series.

2.8.4. Part Manufacturing – Injection Molding

LCI data for injection molding of PA12 is not publicly available. Therefore, this study used general LCI unit process energy data for injection molding from Franklin Associates (2011), shown in **Table 17**.

Table 17. Injection Molding Process LCI (for 1kg part)

Inputs	**Qty**	**Unit**
Materials		
Virgin resin	1.034	kg
Energy		
Electricity	14.3	MJ
Natural gas	0.143	MJ
LPG	0.00381	MJ
Gasoline	0.00067	MJ
Diesel	0.00005	MJ
Total primary energy	14.47	MJ
Emissions		
GHG emissions[a]	1.00	kg CO_2-eq

Note. Material and energy input data are sourced from Franklin Associates (2011), Table 1. LCI Unit Process Data for Injection Molding (p. 19).

[a] Determined primary energy and GHG emissions with GREET1 2019 data for RFC grid, 2020 time series.

3. Results

3.1. HP MJF PA12 Material Yield

Based on the part scrap rate and PA12 powder loss assumptions used in this study, the PA12 material yield of the HP MJF process was 85.8%. In contrast, LCI data from Franklin Associates (2011) indicate a resin-to-product material yield of 96.7% for injection molding. Consequently, injection molding requires 11.3% less PA12 material to produce the same part mass. Considering the modeled PA12 primary energy consumption and GHG emissions LCI data from EarthShift Global, injection molding saves 39 MJ and avoids 1.74 kg CO_2-eq per kg of PA12 parts in comparison to MJF as a direct result of injection molding's superior material yield.
Figure 8 depicts the PA12 material flow and yield across each step of the MJF process.

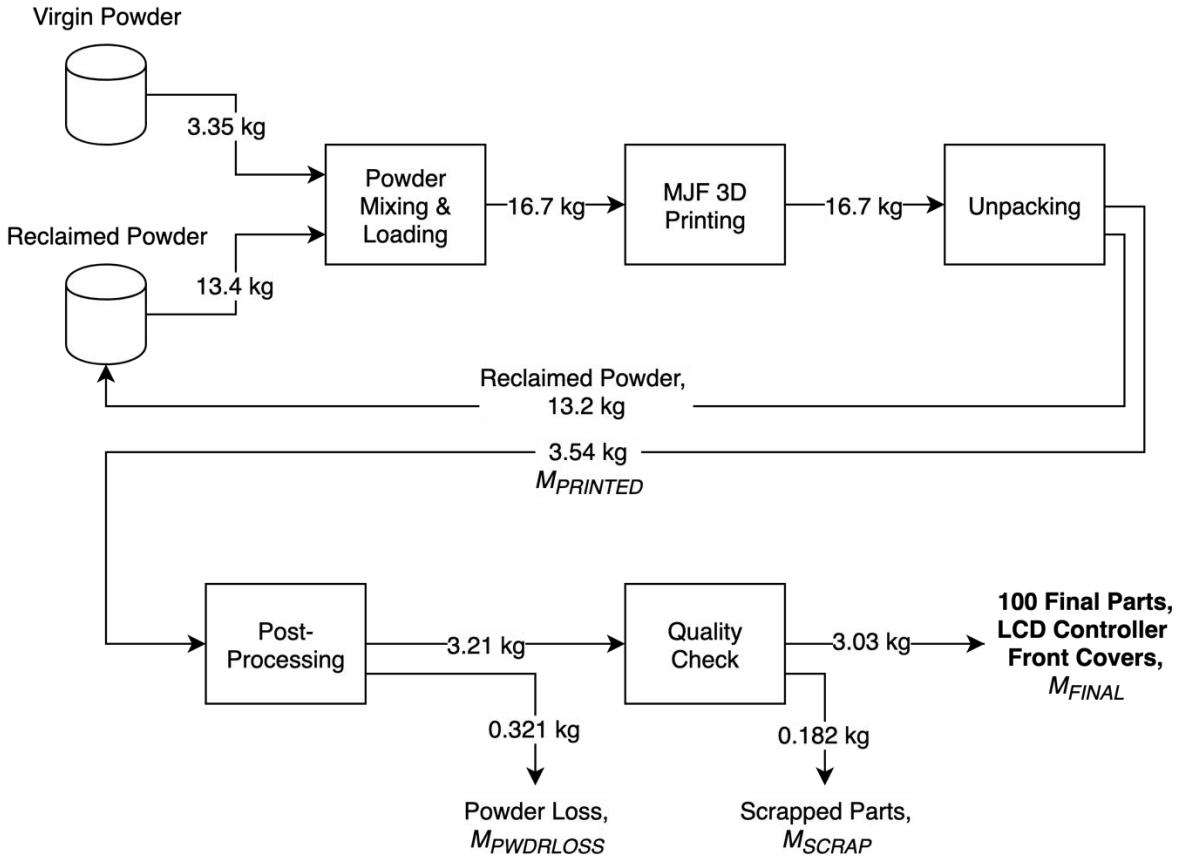

Figure 8. HP MJF PA12 Material Yield Analysis.

The following equations are used to estimate the PA12 material yield of the HP MJF system based on powder loss and scrapped part projections:

(1) $$y_{MJF\_PA12} = \frac{M_{FINAL}}{M_{FINAL}+M_{SCRAP}+M_{PWDRLOSS}} = \frac{M_{FINAL}}{M_{PRINTED}}$$

(2) $$M_{FINAL} = M_{PART} \times Q_{FINAL\_PART}$$

(3) $$M_{SCRAP} = M_{PRINTED} \times r_{SCRAP}$$

(4) $$M_{PRINTED} = M_{PART} \times Q_{PRINTED}$$

(5) $$Q_{PRINTED} = \frac{Q_{FINAL\_PART}}{(1-r_{SCRAP})};\ r_{SCRAP} = \frac{Q_{PRINTED}-Q_{FINAL\_PART}}{Q_{PRINTED}};$$

(6) $$M_{PWDRLOSS} = r_{UNUSABLE} \times (M_{PRINTED})$$

(7) $$r_{UNUSABLE} = \frac{M_{UNUSABLE}}{M_{PART}}$$

where y_{MJF_PA12} is the MJF system's PA12 material yield; M_{FINAL} is the PA12 mass for the desired quantity of final parts; M_{PART} is the PA12 mass of a single part; Q_{FINAL_PART} is the desired quantity of final parts; M_{SCRAP} is the PA12 mass of scrapped parts; $Q_{PRINTED}$ is the quantity of printed parts; r_{SCRAP} is the percentage of parts scrapped due to defects; $M_{PWDRLOSS}$ is the mass of powder loss from post-processing; $M_{UNUSABLE}$ is the amount of unusable powder caked onto parts after unpacking; and $r_{UNUSABLE}$ is the percentage of unusable powder caked onto parts after unpacking, relative to the PA12 mass of an individual part.

The resulting 85.8% PA12 material yield for the MJF process contrasts significantly with yields modeled by studies on SLS discussed in **Section 1.4.4**, which reflect powder waste rates between 20% and 45%.

3.2. Cradle-to-Gate Life Cycle Impact

Production of 100 LCD Controller Front Covers with the HP MJF 3D 4210 Printer results in 2,269 MJ of primary energy consumption and 127 kg CO_2-eq emissions, whereas injection molding with steel tooling results in 8,766 MJ and 569 kg CO_2-eq, and injection molding with aluminum tooling results in 5,258 MJ and 308 kg CO_2-eq. The site energy consumption of the full MJF part manufacturing process, including post-processing, was 152.54 MJ/kg.

Figure 9 shows a comparison of the cradle-to-gate GHG emissions for the three manufacturing processes and the relative contribution of each life cycle phase. The dominant impact for the MJF system is the part manufacturing process. Powder loading and mixing, MJF 3D printing, fast cooling, unpacking, and post-processing account for 56.2% of the cradle-to-gate GHG emissions for the system. In particular, electricity consumption from MJF 3D printing is responsible for 36% of the total system's GHG emissions. The second highest contribution to GHG emissions for the MJF system results from PA12 production with 42.8% of the overall impact. Together, the fusing agent production, detailing agent production, agent transportation, and PA12 transportation accounted for less than 1% of the overall product system GHG emissions.

As expected, the major driver of GHG emissions for injection molding resulted from steel and aluminum plate production, accounting for over 77% of cradle-to-gate GHG emissions. Similarly, PA12 production followed as the second highest contributor to GHG emissions. The injection molding process only accounted for 0.68% of emissions for the manufacturing process with steel tooling and 1.0% of emissions with aluminum tooling. Mold machining accounted for 1.7% of emissions for injection molding with steel tooling, but only accounted for 0.58% with aluminum tooling. PA12 transportation is essentially negligible, accounting for less than 0.1% of cradle-to-gate GHG emissions for injection molding with either type of tooling.

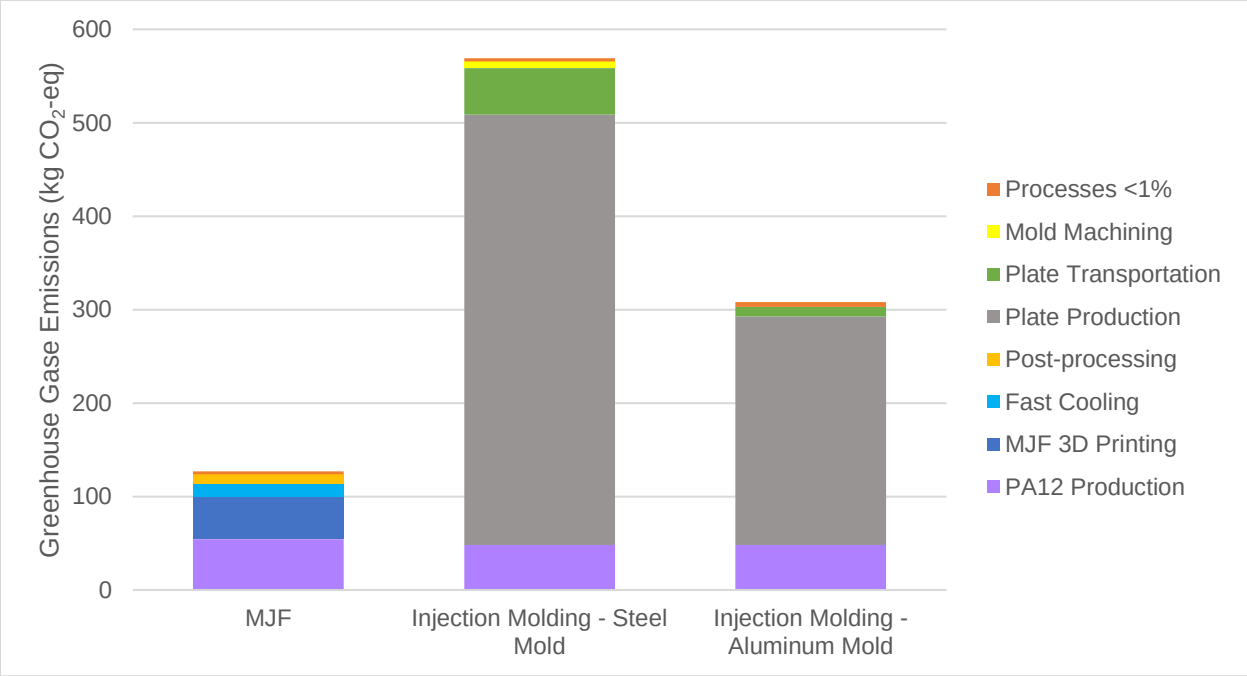

Figure 9. Cradle-to-gate GHG emissions comparison of MJF and injection molding for the functional unit.

The relative contributions of each life cycle phase to the overall cradle-to-gate GHG emissions follow the relative contributions for cradle-to-gate primary energy consumption, but differ slightly for the PA12 production phase. For the MJF LCA, PA12 production accounts for 53.8% of cradle-to-gate primary energy consumption and MJF part manufacturing accounts for 45.3%. Although PA12 production results in fewer GHG emissions than the MJF part manufacturing process, PA12 production is the dominant contributor to cradle-to-gate life cycle primary energy consumption because the ratio of energy consumption to GHG emissions differs for the two phases: 22.4 MJ/kg CO_2-eq for the PA12 production process and 14.4 MJ/kg CO_2-eq for the MJF part manufacturing process. The difference is likely a result of the PA12 material feedstock energy. For example, feedstock energy contributes approximately 30% to the cradle-to-gate primary energy consumption for PA6 production (PlasticsEurope, 2014). The change in relative contribution to cradle-to-gate primary energy consumption is less notable for the injection molding processes due to the much larger impacts of mold plate production. Additional data depicting the cradle-to-gate primary energy consumption for MJF and injection molding are shown in the **Appendix A.1.**

The results for the MJF cradle-to-gate primary energy consumption contribution analysis and MJF part manufacturing process specific energy consumption (SEC) show similarities to previous studies on SLS. The 53.8% contribution of PA12 production to the cradle-to-gate primary energy consumption for the MJF system compares closely to the finding from Telenko and Seepersad (2012) that nylon production accounted for 60.2% of SLS energy consumption. The higher proportion of impact stemming from SLS nylon production can be attributed to the fact that Telenko and Seepersad's (2012) modeled material yield was significantly lower than the material yield in this study. Moreover, Telenko and Seepersad (2012) did not account for the energy consumption associated with cooling, unpacking, and post-processing, as previous studies

on SLS energy consumption also excluded these steps. For an appropriate comparison with SLS, the MJF part manufacturing process SEC, considering only the powder mixing and loading and 3D printing energy consumption, was 98.69 MJ/kg. Consequently, the MJF SEC falls slightly lower than the range of SLS SECs noted in **Section 1.4.2**. **Table A1** in **Appendix A** provides additional data on the SEC value for each step of the MJF part manufacturing process.

3.3. Greenhouse Gas Emissions by Production Volume

Despite the lower GHG emissions for production of the functional unit, the MJF system's GHG emissions quickly rises as production volume increases. In contrast, GHG emissions for injection molding with either type of tooling rises at a much slower rate because the one-time impact from plate production and plate transportation amortizes over larger quantities of LCD controller front cover parts. **Figure 10** shows the GHG emissions per part of each manufacturing process for quantities ranging from 100 to 1,000 parts. The MJF system maintains a lower emissions per part ratio relative to injection molding with steel tooling up to a quantity of approximately 800 parts. The breakeven emissions per part ratio between the MJF system and injection molding with aluminum tooling occurs at approximately 450 parts. **Figure A5** in **Appendix A** provides additional GHG emissions results data for production volumes up to 5,000 parts. At a production volume of 3,000 parts, the MJF system produces double the GHG emissions of injection molding with aluminum tooling.

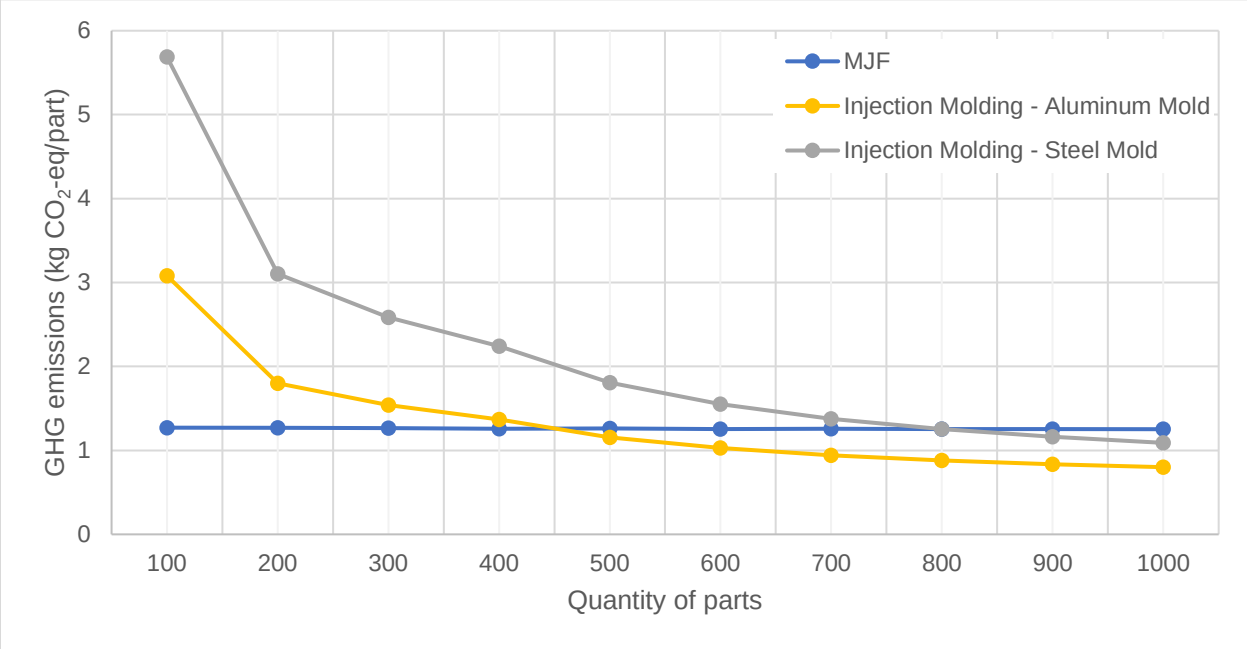

Figure 10. Comparison of GHG emissions per LCD controller front cover part by production volume for MJF 3D printing and injection molding. Part manufacturing electricity sourced from U.S. RFC grid.

3.4. Sensitivity Analysis

3.4.1. Solar-Powered Manufacturing Facility

Based on the high electricity consumption of the HP MJF process, this study analyzed how a difference in the source of electricity generation for the manufacturing facility would alter the GHG emissions breakeven point with injection molding.

Figure 11 shows the GHG emissions per part produced by each manufacturing process for quantities ranging from 2,000 to 10,000 parts in a scenario with the part manufacturing facility powered by a photovoltaic (PV) system instead of the U.S. RFC electric grid. In this scenario, the MJF system maintains a lower emissions per part ratio relative to injection molding with steel tooling up to a quantity of approximately 7,500 parts. The breakeven emissions per part ratio between the MJF system and injection molding with aluminum tooling occurs at approximately 3,750 parts.

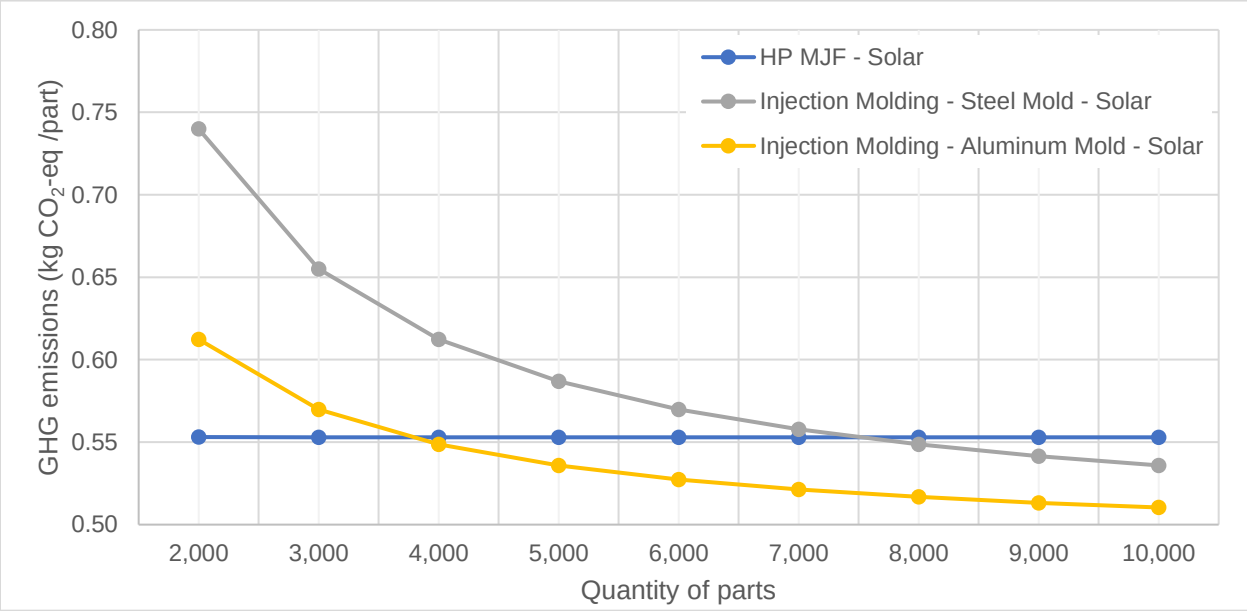

Figure 11. Comparison of GHG emissions per part by production volume for MJF 3D printing and injection molding. Part manufacturing electricity sourced from photovoltaic power plant.

Despite zero emissions associated with powering the part manufacturing facility, the MJF system ultimately results in greater GHG emissions than injection molding because of the system's lower PA12 material yield. Together, the relatively high emissions from the PA12 production phase and the lower PA12 material yield limit the breakeven production volume of the MJF system.

3.4.2. Material Yield

Given the uncertainty associated with the MJF process scrap rate and powder recovery rate, this study used a sensitivity analysis to explore the variance in GHG emissions resulting from different material yields. **Figure 12** shows the cradle-to-gate GHG emissions from the MJF process across different material yields using the reported PA12 LCI data and electricity sourced from a PV power plant. Under the solar-powered manufacturing facility condition and a 10% decrease in material yield to 77.2%, the MJF process emits fewer GHGs than injection molding

with aluminum tooling until a production volume of approximately 1,000 parts. In contrast, an improvement in material yield by 10% to 94.3% results in a breakeven point between the MJF process and injection molding near a quantity of 10,000 parts. This material yield is insufficient for the MJF process to achieve lower GHG emissions than injection molding much farther beyond 10,000 parts because injection molding maintains a higher material yield. Moreover, as production quantity increases, the marginal increase in GHG emissions from fusing agent and detailing agent production and transportation outweighs the marginal increase in GHG emissions from injection molding.

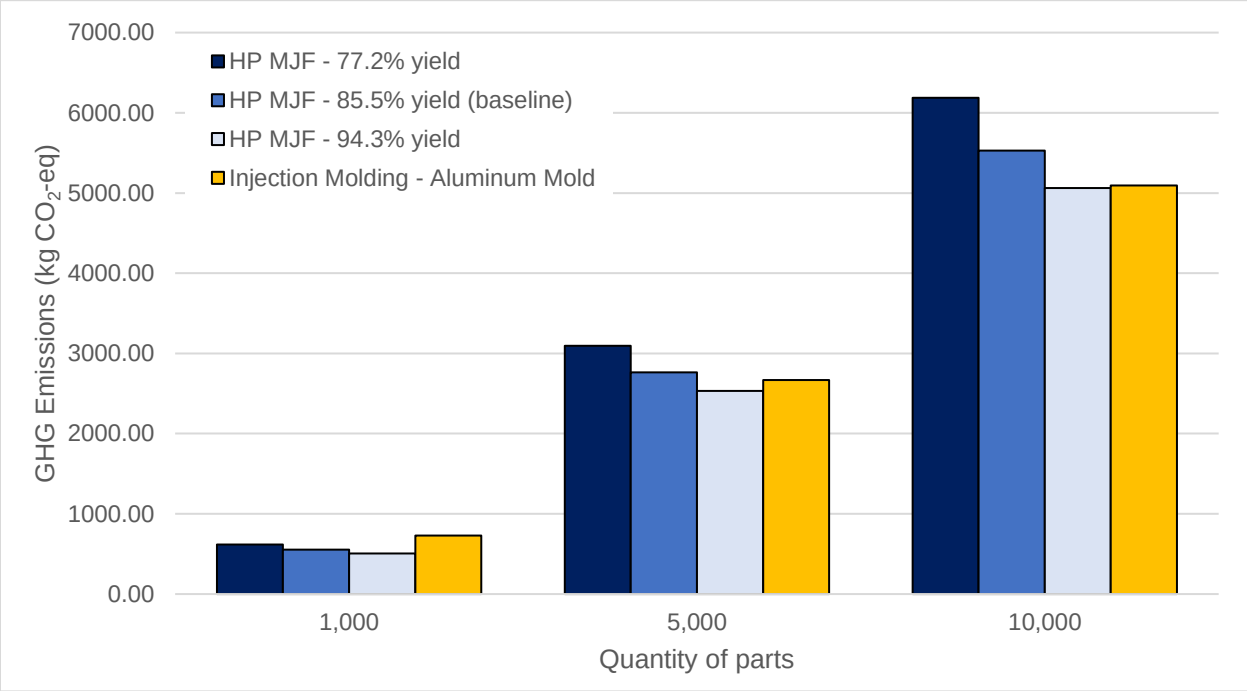

Figure 12. PA12 material yield sensitivity analysis, electricity sourced from photovoltaic power plant.

3.4.3. PA12 Production LCI

Considering the uncertainty of the LCI data for PA12 production and the use of PA6 as a substitute in other additive manufacturing LCAs, this study assessed how the variance in raw material modeling assumptions would affect the GHG emissions results of MJF and injection molding with aluminum tooling. **Figure 13** shows the GHG emissions of the HP MJF process and injection molding with aluminum tooling using the PlasticsEurope PA6 LCI data under the condition where electricity is sourced from a PV power plant. In this scenario, the MJF breakeven GHG emissions shifts to a point between 5,000 and 10,000 parts for injection molding with aluminum tooling and a point between 10,000 and 15,000 parts for injection molding with steel tooling. The lower energy demand associated with the PA6 noticeably lessens the negative impact of the HP MJF's material yield.

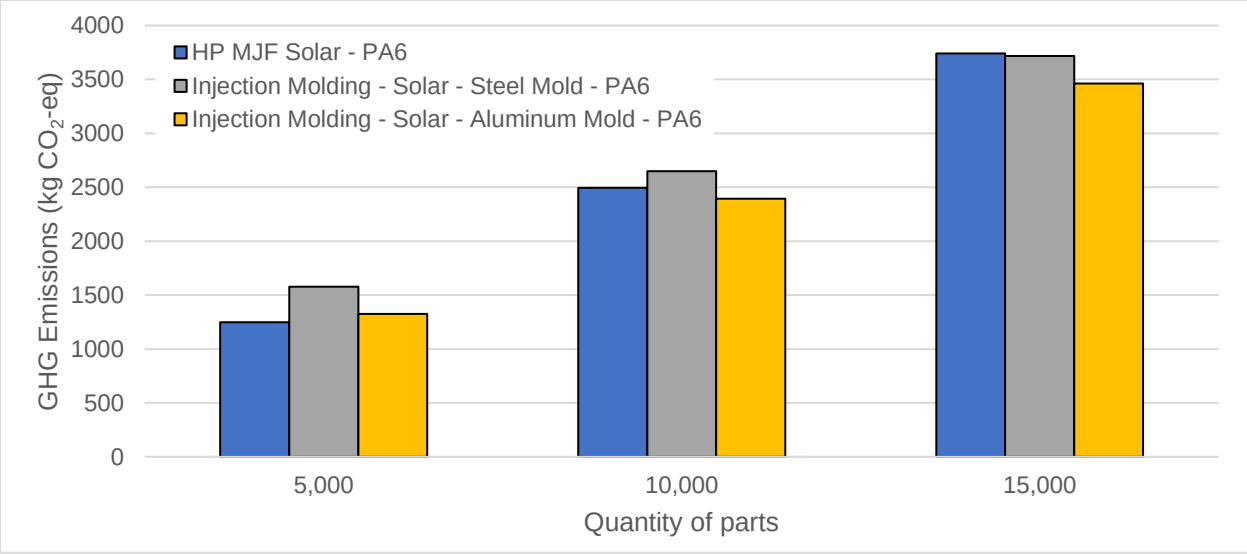

Figure 13. PA12 production LCI sensitivity analysis, electricity sourced from photovoltaic power plant.

3.4.4. Post-Processing Time.

A sensitivity analysis of post-processing time variance was conducted to evaluate the corresponding effects on cradle-to-gate GHG emissions for the MJF process. **Figure 14** shows the cradle-to-gate GHG emissions for the MJF process with three scenarios for post-processing: 1 minute of blasting, 3 minutes of blasting, and 5 minutes of blasting. The results show that a relatively minor increase in the amount of blasting time for each part significantly increases the cradle-to-gate GHG emissions for the MJF process. With 5 minutes of blasting per part, the MJF process would no longer breakeven with injection molding at a quantity of 250 parts.

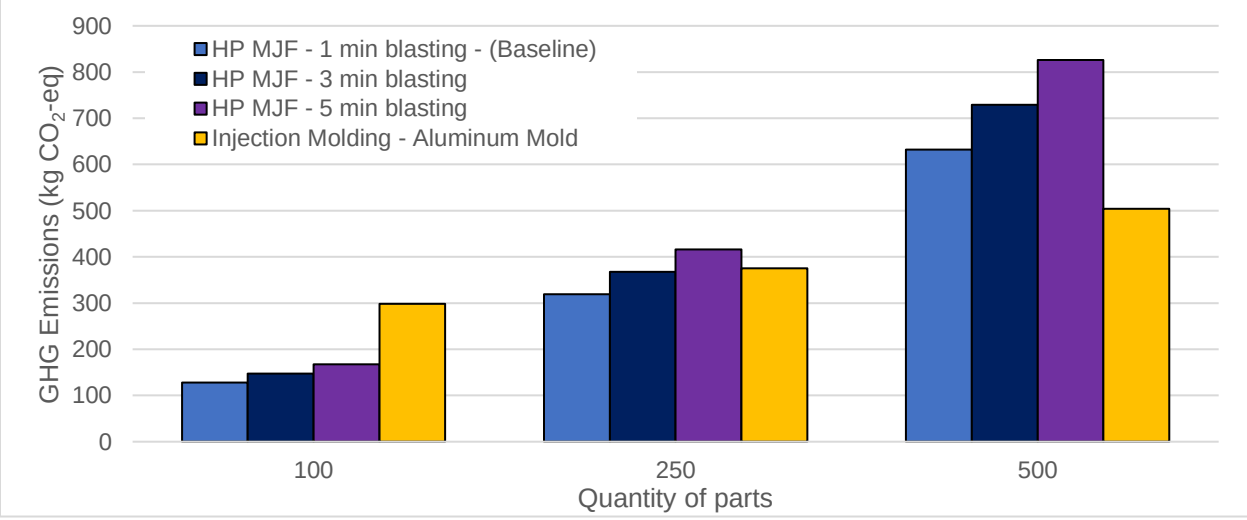

Figure 14. Post-processing time sensitivity analysis, electricity sourced from RFC grid.

3.4.5. Variable Sensitivity.

The source of electricity generation for part manufacturing plays the largest role in determining the GHG emissions of the MJF system as shown in **Figure 15**. Shifting electricity generation to a renewable source from the U.S. RFC grid can reduce the GHG emissions of the functional unit

by 56%. Post-processing time, PA12 production LCI, and printing speed can cause the MJF GHG emissions to change by over 20%.

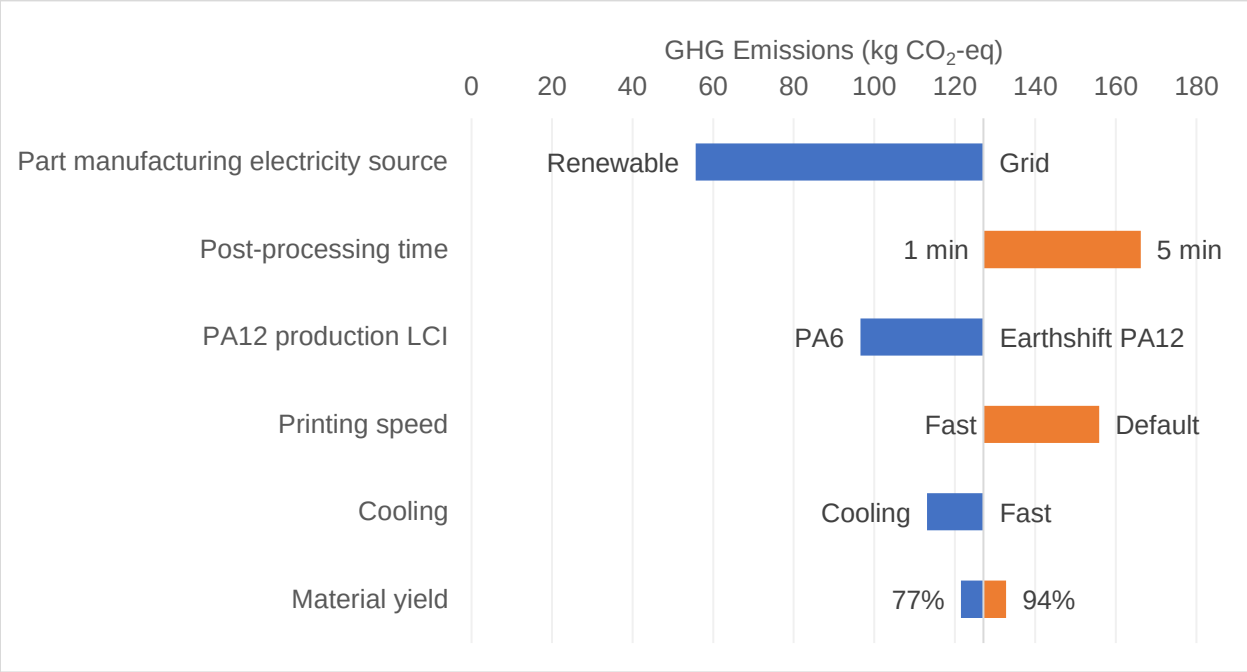

Figure 15. Variable sensitivity analysis.

4. Discussion

The results from this study show that the process energy consumption of MJF is slightly lower than the range of SLS values in the literature when excluding steps that were not examined in previous studies. Including all process steps in the MJF SEC still places MJF in the SLS SEC range. This finding indicates MJF is marginally more energy efficient than SLS, more energy efficient than FDM, and less energy efficient than some forms of SLA (Kellens, Mertens, et al., 2017). However, the powder loss and scrap rates modeled in this study result in a higher resource efficiency for MJF in comparison to SLS, signifying a potentially lower overall environmental impact for the MJF process. Considering the 45% powder waste material rate from Kellens et al. (2014) and a conservative estimate for PA12 embodied energy of 129.1 MJ/kg, SLS would consume 84 MJ more than MJF per kilogram of final product as a result of SLS's lower resource efficiency. Although MJF requires fusing agent and detailing agent not used in SLS, these consumables only amount to 5.8 MJ per kilogram of final product.

Despite MJF's resource efficiency advantage over SLS, MJF consumes more primary energy and causes more indirect GHG emissions than injection molding for large production volumes. For the part design and conditions modeled in this study, MJF results in lower primary energy consumption and GHG emissions than injection molding across low production volumes (450 to 800 parts). Beyond 450 to 800 parts, the environmental impact of MJF substantially exceeds injection molding with either type of tooling. This finding is consistent with previous studies that compared SLS to injection molding (Telenko & Seepersad, 2012; Chen et al., 2015).

Results from the sensitivity analyses show that changes to several variables can significantly influence the GHG emissions breakeven point between MJF and injection molding. Varying the source of electricity for the manufacturing facility, the amount of time spent air/bead blasting, the LCI data used for PA12 production, and the printing speed can alter the GHG emissions breakeven point between MJF and injection molding by over 20%. A scenario with each of these variables set to the optimum condition for MJF could shift the GHG emissions breakeven point between MJF and injection molding to 5,000 to 10,000 parts.

Smaller parts could result in higher breakeven production volumes (Telenko & Seepersad, 2012). Despite a potentially higher quantity of parts in a full build chamber with a smaller part size and higher packing, the cradle-to-gate GHG emissions of the MJF process would surpass injection molding between 5 and 8 print jobs. Furthermore, modifications to the mold design, such as increasing the number of cavities, could counter the optimal conditions for MJF and further reduce the GHG emissions breakeven point for higher volumes.

Although the part simulated in this study resulted in a relatively low GHG emissions breakeven point between MJF and injection molding, the design capabilities of MJF and other additive manufacturing technologies permit the production of parts that could not otherwise be manufactured with injection molding. In such cases, there is no GHG emissions breakeven point unless an alternate injection molding-capable design (perhaps comprising several injection-moldable components) could be aptly substituted for the original part design.

4.1. Limitations

The part design, packing method, MJF LCI data, and quality assumptions limit the generalization of this study's findings across other applications. Only one part design was considered in this study, but different part designs could change the environmental impact associated with injection molding and the resulting breakeven point with MJF. Moreover, this study applied an automated packing method from Autodesk Netfabb that does not incorporate the ability to nest parts within the build, resulting in a relatively low packing density of 8.1%. Nesting parts appropriately could increase the packing density and result in a lower ratio of energy consumption to parts produced (Telenko & Seepersad, 2012). Finally, the electricity and material consumption data and assumptions used in this study for the MJF process were not experimentally validated. Similarly, direct process emissions for the MJF process were not investigated.

4.2. Recommendations for Future Research

4.2.1. PA12 Production LCI

As shown in this study, the selected LCI data for PA12 production can result in significantly different breakeven points between MJF and injection molding. Considering the prominent use of PA12 as an additive manufacturing material and rapid growth of the industry, future research should publish LCI data for PA12 production.

4.2.2. MJF Electricity Consumption Profile, Direct Emissions, and Material Yield

This study modeled the energy consumption and material yield of the MJF process based on data and assumptions drawn from MJF technical documents and communications with HP employees. However, subsequent research should develop an accurate electricity consumption profile of the MJF process for both the printer and the processing station to understand how energy use

fluctuates over the course of powder loading and mixing, printing, fast cooling, and unpacking. Similarly, the material yield of the MJF process should be validated across different part designs and volumes. Finally, the direct emissions of the MJF process should be examined in future research.

4.2.3. Post-Processing Methods

Post-processing is a non-trivial step in the MJF process. Considering the high energy consumption associated with compressed air systems, this step can significantly alter the environmental impact of parts production with MJF. Future research should investigate the time and environmental impact of different post-processing methods applied to a variety of part designs.

5. Conclusion

This study provided a cradle-to-gate life cycle assessment of primary energy consumption and GHG emissions for MJF. As applied to this study's representative part, the LCA showed that the SEC of MJF is marginally lower than SLS. Moreover, the modeled powder loss and scrap rate resulted in a material yield much higher than SLS, indicating an overall lower environmental impact for MJF. Consequently, MJF presents both cost and sustainability advantages over SLS in cases where both processes could be used to produce the same part.

This LCA also demonstrated that MJF consumes less energy and results in fewer GHG emissions than injection molding with steel or aluminum tooling for low production volumes, though the breakeven production volume for GHG emissions is much smaller than the economic breakeven production volumes asserted by HP. After approximately 5 to 8 print jobs, the MJF environmental impact begins to exceed that of injection molding. This breakeven point fluctuates significantly based on the electricity generation source, post-processing time, PA12 production emissions intensity, and printing speed. Powering the part manufacturing facility from renewable electricity sources can increase the GHG emissions breakeven quantity of MJF with injection molding by an order of magnitude, but ultimately crosses over due to MJF's lower material yield. On the basis of sustainability, this study shows that MJF 3D printing causes less environmental harm than injection molding for low production volumes, but cannot yet displace large-scale production of plastics parts that are capable of being injection molded without environmental tradeoffs.

Appendix A

A.1. Cradle-to-Gate Primary Energy Consumption Results

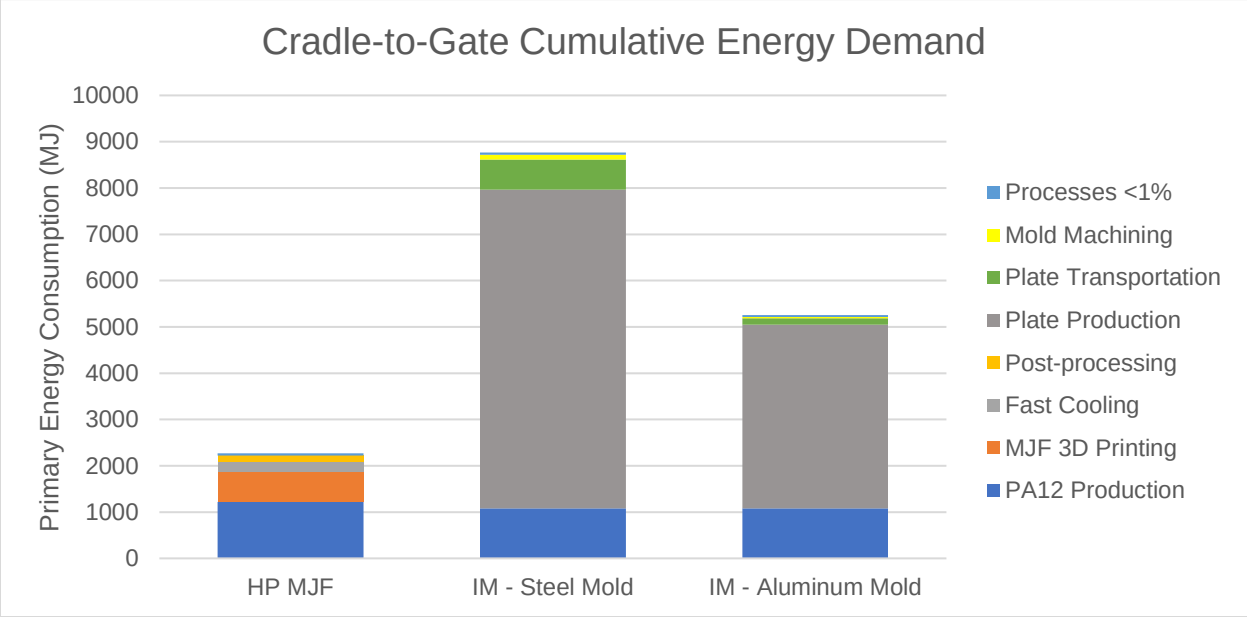

Figure A1. Cradle-to-gate primary energy consumption comparison of MJF and injection molding for the production of 100 LCD controller front cover parts.

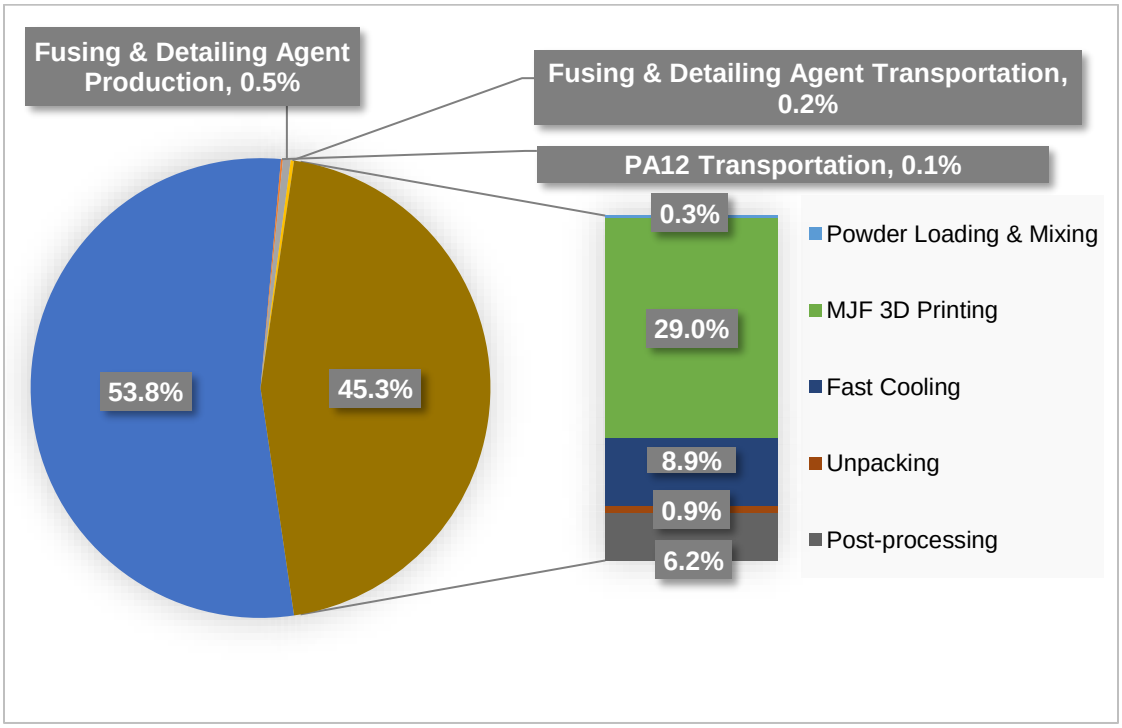

Figure A2. MJF cradle-to-gate primary energy consumption contribution analysis.

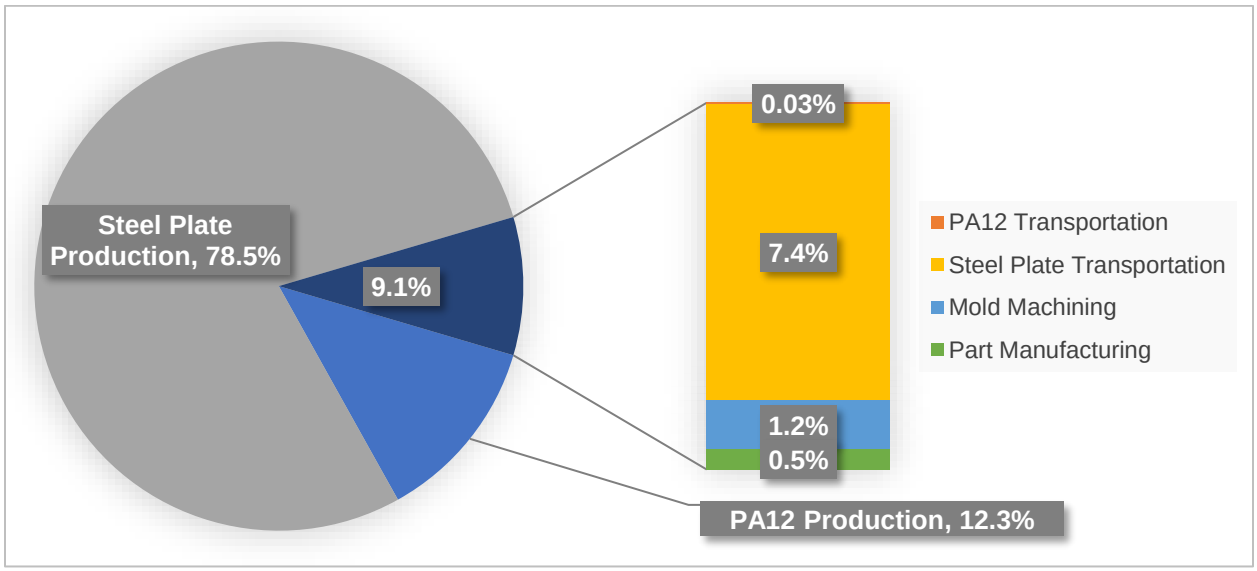

Figure A3. Injection molding with steel tooling cradle-to-gate primary energy consumption contribution analysis

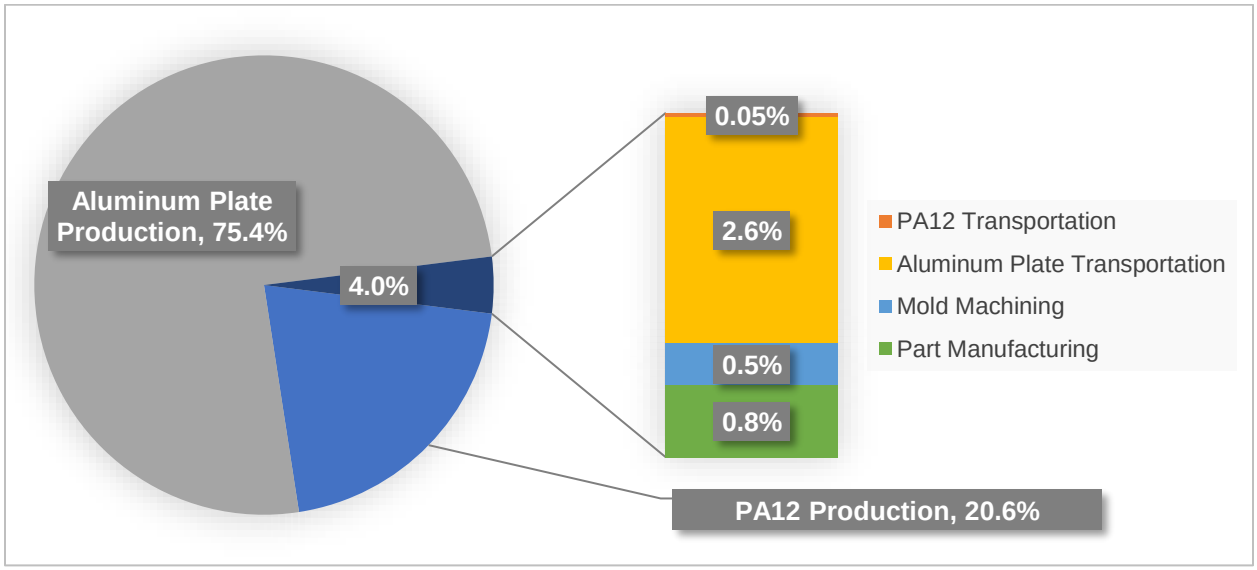

Figure A4. Injection molding with aluminum tooling cradle-to-gate primary energy consumption contribution analysis

Table A1. MJF Part Manufacturing Specific Energy Consumption per kg PA12

MJF Part Manufacturing Process Step	SEC (MJ/kg)
Powder mixing & loading	1.05
MJF 3D printing	97.64
Fast Cooling	29.96
Unpacking	3.09
Post-processing	20.86
Total SEC	**152.54**
Total SEC (including powder mixing, loading and MJF 3D printing only)	**98.69**

A.2. Greenhouse Gas Emissions by Production Volume Results

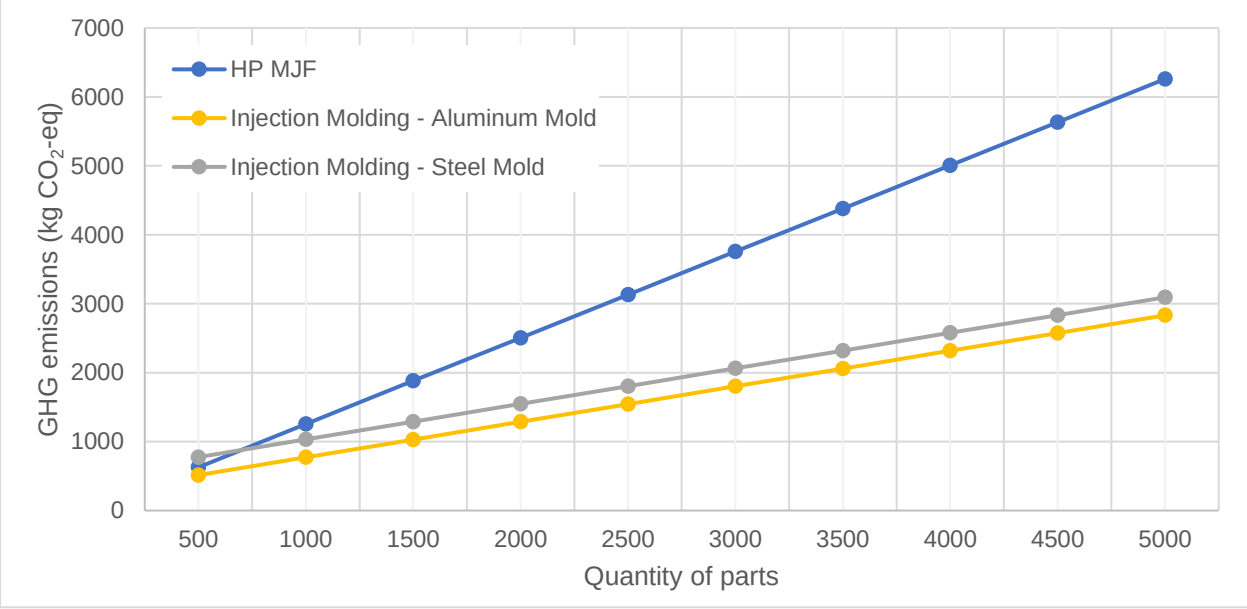

Figure A5. GHG emissions by production volume comparison for MJF and injection molding.

References

American Metal Market. (2018). *North American Steel Producers 2018*. Retrieved from https://www.steel.org/-/media/doc/steel/policy/member-states/amm-steel-producers-map-2018.ashx?la=en&hash=E07E05F73CF2B67381AF97058651FA55CA99D240

ArcelorMittal USA. (2015). *Plate: MTD and Tool Steels: for Mold, Tool and Die Applications*.

Argonne National Laboratory. (2019a). *The Greenhouse Gases, Regulated Emissions, and Energy Use in Transportation (GREET) Model Software: GREET Version 1_2019*. Retrieved from https://greet.es.anl.gov/greet_1_series

Argonne National Laboratory. (2019b). *The Greenhouse Gases, Regulated Emissions, and Energy Use in Transportation (GREET) Model Software: GREET Version 2_2019*.

ASTM International. (2015). *ISO/ASTM52900-15 Standard Terminology for Additive Manufacturing - General Principles - Terminology*. Retrieved from https://doi-org.proxy.lib.umich.edu/10.1520/ISOASTM52900-15

ATHENA Sustainable Materials Institute. (2002). *Cradle-To-Gate Life Cycle Inventory : Canadian and US Steel Production by Mill Type*. Retrieved from http://www.athenasmi.org/wp-content/uploads/2011/10/1_Steel_Production.pdf

Autodesk Inc. (2020a). About Packing | Netfabb 2019 | Autodesk Knowledge Network. Retrieved March 15, 2020, from https://knowledge.autodesk.com/support/netfabb/learn-explore/caas/CloudHelp/cloudhelp/2019/ENU/NETF/files/GUID-52326727-C6CE-44DA-ACC3-7BBBFF7694DC-htm.html

Autodesk Inc. (2020b). Working with 3D Packing - Monte Carlo | Netfabb 2019 | Autodesk Knowledge Network. Retrieved March 15, 2020, from https://knowledge.autodesk.com/support/netfabb/learn-explore/caas/CloudHelp/cloudhelp/2019/ENU/NETF/files/GUID-BEB7771C-1C95-4280-8E4B-EAAAD5ED66F7-htm.html

Back, A. (2019). HP's MJF: The fastest growing 3D Printing Process of 2019. Retrieved April 17, 2020, from 3D Hubs website: https://www.3dhubs.com/blog/mjf-fastest-growing-3d-printing-process/

Bain, E. D. (2019). Polymer Powder Bed Fusion Additive Manufacturing: Recent Developments in Materials, Processes, and Applications [Chapter]. *ACS Symposium Series*, *1315*, 7–36. https://doi.org/10.1021/bk-2019-1315.ch002

Baumers, M., Tuck, C., Bourell, D. L., Sreenivasan, R., & Hague, R. (2011). Sustainability of additive manufacturing: Measuring the energy consumption of the laser sintering process. *Proceedings of the Institution of Mechanical Engineers, Part B: Journal of Engineering Manufacture*, *225*(12), 2228–2239. https://doi.org/10.1177/0954405411406044

Baumers, M., Tuck, C., Wildman, R., Ashcroft, I., & Hague, R. (2011). Energy inputs to additive manufacturing: does capacity utilization matter? *Proceedings of the 23rd Solid Freeform Fabrication Symposium 2011*, 30–40.

Boothroyd, G., Dewhurst, P., & Knight, W. A. (2010). Design for Injection Molding. In *Product Design for Manufacture and Assembly* (3rd ed., pp. 331–374). https://doi.org/10.1201/9780824741587.ch8

Bours, J., Adzima, B., Gladwin, S., Cabral, J., & Mau, S. (2017). Addressing Hazardous Implications of Additive Manufacturing: Complementing Life Cycle Assessment with a Framework for Evaluating Direct Human Health and Environmental Impacts. *Journal of Industrial Ecology*, *21*, S25–S36. https://doi.org/10.1111/jiec.12587

Butler, J. (2011). Using selective laser sintering for manufacturing. *Assembly Automation*, *31*(3), 212–219. https://doi.org/10.1108/01445151111150541

Campo, E. A. (2006). Injection Mold Design. In *Complete Part Design Handbook - For Injection Molding of Thermoplastics* (pp. 545–592). Retrieved from https://app.knovel.com/hotlink/pdf/id:kt004X3QV8/complete-part-design/classification-injection

Chen, D., Heyer, S., Ibbotson, S., Salonitis, K., Steingrímsson, J. G., & Thiede, S. (2015). Direct digital manufacturing: Definition, evolution, and sustainability implications. *Journal of Cleaner Production*, *107*, 615–625. https://doi.org/10.1016/j.jclepro.2015.05.009

Christou, M. (2013). Case for the Full Graphic Smart LCD Controller by wersy. Retrieved from Thingiverse website: https://www.thingiverse.com/thing:87250

Clemco Industries Corp. (2007). Compressed-Air and Abrasive Consumption. Retrieved April 17, 2020, from https://clemcoindustries.com/info-tools/compressed-air-and-abrasive-consumption-estimates/

Dahmus, J. B., & Gutowski, T. G. (2004). An environmental analysis of machining. *American Society of Mechanical Engineers, Manufacturing Engineering Division, MED*, *15*, 643–652. https://doi.org/10.1115/IMECE2004-62600

Davies, S. (2017). HP launches 4210 Multi Jet Fusion platform offering 110k breakeven point vs injection moulding. *TCT Magazine*. Retrieved from https://www.tctmagazine.com/3d-printing-news/hp-4210-multi-jet-fusion-platform-110k-breakeven-point/

Devaux, J., Lê, G., & Pees, B. (n.d.). *Application of Eco-Profile Methodology To Polyamide 11*. Retrieved from https://www.extrememateriales-arkema.cn/export/sites/technicalpolymers/.content/medias/downloads/article-reprints/rilsan-article-reprints/RilsanFamily_eco-profile_article.pdf

Distances & Time. (n.d.). Retrieved April 15, 2020, from https://www.searates.com/services/distances-time/

DME Company. (2020). *DME XPress ™ A-Series Mold Base*. Retrieved from https://dme.net/wp-content/uploads/ProductSheets/XPress_XPA_MoldBases-v5_14.pdf

Dotchev, K., & Yusoff, W. (2009). Recycling of polyamide 12 based powders in the laser sintering process. *Rapid Prototyping Journal*, *15*(3), 192–203. https://doi.org/10.1108/13552540910960299

Emamjomeh, A., Prasad, K. A., Novick, M. A., & Fung, E. M. (2019). *Patent No. 10,392,512 B2*. Washington, DC: U.S. Patent and Trademark office.

EOS GmbH Electro Optical Systems. (n.d.). Polymer Material Management for industrial 3D Printing. Retrieved April 14, 2020, from https://www.eos.info/material-management-plastic

Evonik Resource Efficiency GmbH. (n.d.-a). High performance plastic powder materials for 3d printing - Evonik Industries AG. Retrieved January 8, 2020, from https://3d-printing.evonik.com/product/additive-manufacturing/en/materials/polymer-powders/

Evonik Resource Efficiency GmbH. (n.d.-b). VESTAMID® L - VESTAMID®—A history of the evolution of high-performance polyamides. Retrieved January 8, 2020, from https://www.vestamid.com/product/vestamid/en/products-services/vestamid-l/

Faludi, J., Baumers, M., Maskery, I., & Hague, R. (2017). Environmental Impacts of Selective Laser Melting: Do Printer, Powder, Or Power Dominate? *Journal of Industrial Ecology*, *21*, S144–S156. https://doi.org/10.1111/jiec.12528

Fischedick, M., Roy, J., Abdel-Aziz, A., Acquaye, A., Allwood, J. M., Ceron, J.-P., … Tanaka, K. (2014). Industry. In O. Edenhofer, R. Pichs-Madruga, Y. Sokona, E. Farahani, S.

Kadner, K. Seyboth, … J. C. Minx (Eds.), *Climate Change 2014: Mitigation of Climate Change. Contribution of Working Group III to the Fifth Assessment Report of the Intergovernmental Panel on Climate Change* (pp. 1–110). Retrieved from Cambridge University Press, Cambridge, United Kingdom and New York, NY, USA

Ford, S., & Despeisse, M. (2016). Additive manufacturing and sustainability: an exploratory study of the advantages and challenges. *Journal of Cleaner Production, 137*, 1573–1587. https://doi.org/10.1016/j.jclepro.2016.04.150

Franklin Associates. (2011). *LIFE CYCLE INVENTORY OF PLASTIC FABRICATION PROCESSES: INJECTION MOLDING AND THERMOFORMING*. Retrieved from https://plastics.americanchemistry.com/Education-Resources/Publications/LCI-of-Plastic-Fabrication-Processes-Injection-Molding-and-Thermoforming.pdf

Goodridge, R. D., Tuck, C. J., & Hague, R. J. M. (2012). Laser sintering of polyamides and other polymers. *Progress in Materials Science, 57*(2), 229–267. https://doi.org/10.1016/j.pmatsci.2011.04.001

Gutowski, T., Dahmus, J., & Thiriez, A. (2006). Electrical Energy Requirements for Manufacturing Processes. *Energy*, *2*(Cvd), 623–628. Retrieved from http://web.mit.edu/ebm/www/Publications/CIRP_2006.pdf

Gutowski, T., Jiang, S., Cooper, D., Corman, G., Hausmann, M., Manson, J. A., … Sekulic, D. P. (2017). Note on the Rate and Energy Efficiency Limits for Additive Manufacturing. *Journal of Industrial Ecology*, *21*, S69–S79. https://doi.org/10.1111/jiec.12664

Heikoff, W. (2019). *IBISWorld Industry Report OD4428: 3D Printer Manufacturing in the US*.

Hopkinson, N., Hague, R. J. M., & Dickens, P. M. (2006). Rapid Manufacturing: An Industrial Revolution for the Digital Age. In *Rapid Manufacturing: An Industrial Revolution for the Digital Age*. https://doi.org/10.1002/0470033991

HP Development Company L.P. (n.d.). HP 3D Jet Fusion 4200 - Commercial & Industrial 3D Printer. Retrieved April 14, 2020, from https://www8.hp.com/us/en/printers/3d-printers/products/multi-jet-fusion-4200.html

HP Development Company L.P. (2017a). *HP Accelerates Path to Industrial 3D Manufacturing with New Jet Fusion 3D 4210 Printing Solution and Expanded Materials Portfolio*. Retrieved from https://press.ext.hp.com/us/en/press-releases/2017/hp-accelerates-path-to-industrial-3d-manufacturing-with-new-jet-.html

HP Development Company L.P. (2017b). *Technical White Paper: Air Blasting post-process*. Retrieved from https://interpromodels.com/wp-content/uploads/2018/05/White-paper-Air-blasting.pdf

HP Development Company L.P. (2018a). *How To Use Bead Blasting and Post-Processing Techniques | HP Jet Fusion 300 and 500 | HP*.

HP Development Company L.P. (2018b). *HP Jet Fusion Consumables - Country of Origin*. Retrieved from http://h10032.www1.hp.com/ctg/Manual/c06180816

HP Development Company L.P. (2018c). *Technical white paper: HP Multi Jet Fusion technology*.

HP Development Company L.P. (2019a). HP and Smile Direct Club Collaborate on Largest Multi Jet Fusion 3D Production Factory in the U.S. Retrieved October 22, 2019, from https://press.ext.hp.com/us/en/press-releases/2019/hp-and-smile-direct-club-collaborate-on-largest--multi-jet-fusion-3d-production-factory-in-the-us.html

HP Development Company L.P. (2019b). *HP Jet Fusion 3D 4210 Printing Solution*. Retrieved from http://h20195.www2.hp.com/v2/GetDocument.aspx?docname=4AA6-4892ESE

HP Development Company L.P. (2019c). *HP Jet Fusion 4200 3D Printing Solution User Guide*. Retrieved from http://h20195.www2.hp.com/v2/GetDocument.aspx?docname=4AA6-4892ESE

HP Development Company L.P. (2019d). HP Propelling Industry to 3D Production. Retrieved October 22, 2019, from https://press.ext.hp.com/us/en/press-releases/2019/hp-propelling-industry-to-3d-production--more-than-10-million-pa.html

HP Development Company L.P. (2020a). *HP 3D Printing materials*. Retrieved from https://h20195.www2.hp.com/v2/getpdf.aspx/4AA7-1533ENA.pdf

HP Development Company L.P. (2020b). *Safety Data Sheet: V1Q60Series*. Retrieved from http://h22235.www2.hp.com/hpinfo/globalcitizenship/environment/productdata/Countries/us/3d_v1q60series_us_eng_v47.pdf

HP Development Company L.P. (2020c). *Safety Data Sheet: V1Q61Series*. Retrieved from http://h22235.www2.hp.com/hpinfo/globalcitizenship/environment/productdata/Countries/us/3d_v1q61series_us_eng_v37.pdf

Huang, Y., Leu, M. C., Mazumder, J., & Donmez, A. (2015). Additive manufacturing: Current state, future potential, gaps and needs, and recommendations. *Journal of Manufacturing Science and Engineering, Transactions of the ASME*, *137*(1), 1–10. https://doi.org/10.1115/1.4028725

International Organization for Standardization. (2006). *Environmental management — Life cycle assessment — Principles and framework (ISO 14040:2006)*. https://doi.org/10.1016/j.ecolind.2011.01.007

Kazmer, D. O. (2016a). Mold Cost Estimation. *Injection Mold Design Engineering*, 43–78. https://doi.org/10.3139/9781569905715.003

Kazmer, D. O. (2016b). Mold Layout Design. In *Injection Mold Design Engineering* (pp. 79–107). https://doi.org/10.3139/9781569905715.004

Kellens, K., Yasa, E., Renadli, Dewulf, W., Kruth, J. P., & Duflou, J. R. (2011). Energy and Resource Efficiency of SLS/SLM Processes. *Proceedings of the 23rd Solid Freeform Fabrication Symposium 2011*. https://doi.org/10.16194/j.cnki.31-1059/g4.2011.07.016

Kellens, Karel, Baumers, M., Gutowski, T. G., Flanagan, W., Lifset, R., & Duflou, J. R. (2017). Environmental Dimensions of Additive Manufacturing: Mapping Application Domains and Their Environmental Implications. *Journal of Industrial Ecology*, *21*(S1), S49–S68. https://doi.org/10.1111/jiec.12629

Kellens, Karel, Mertens, R., Paraskevas, D., Dewulf, W., & Duflou, J. R. (2017). Environmental Impact of Additive Manufacturing Processes: Does AM contribute to a more sustainable way of part manufacturing? *Procedia CIRP*, *61*, 582–587. https://doi.org/10.1016/j.procir.2016.11.153

Kellens, Karel, Renaldi, R., Dewulf, W., Kruth, J. P., & Duflou, J. R. (2014). Environmental impact modeling of selective laser sintering processes. *Rapid Prototyping Journal*, *20*(6), 459–470. https://doi.org/10.1108/RPJ-02-2013-0018

Kruth, J. P., Levy, G., Klocke, F., & Childs, T. H. C. (2007). Consolidation phenomena in laser and powder-bed based layered manufacturing. *CIRP Annals - Manufacturing Technology*, *56*(2), 730–759. https://doi.org/10.1016/j.cirp.2007.10.004

Krystofik, M., Babbitt, C. W., & Gaustad, G. (2014). When consumer behavior dictates life cycle performance beyond the use phase: Case study of inkjet cartridge end-of-life management. *International Journal of Life Cycle Assessment*, *19*(5), 1129–1145. https://doi.org/10.1007/s11367-014-0713-6

Ligon, S. C., Liska, R., Stampfl, J., Gurr, M., & Mülhaupt, R. (2017). Polymers for 3D Printing and Customized Additive Manufacturing. *Chemical Reviews*, *117*(15), 10212–10290. https://doi.org/10.1021/acs.chemrev.7b00074

Linear AMS. (n.d.). Retrieved from https://www.linearams.com

Luo, Y., Ji, Z., Leu, M. C., & Caudill, R. (1999). Environmental performance analysis of solid freeform fabrication processes. *IEEE International Symposium on Electronics and the Environment*, 1–6. https://doi.org/10.1109/isee.1999.765837

Mani, M., Lyons, K. W., & Gupta, S. K. (2014). Sustainability characterization for additive manufacturing. *Journal of Research of the National Institute of Standards and Technology*, *119*, 419–428. https://doi.org/10.6028/jres.119.016

Mansour, S., & Hague, R. (2003). Impact of rapid manufacturing on design for manufacture for injection moulding. *Proceedings of the Institution of Mechanical Engineers, Part B: Journal of Engineering Manufacture*, *217*(4), 453–461. https://doi.org/10.1243/095440503321628134

Marshall, R., Scales, W., Shafer, G., Shaw, P., Sheaffer, P., Stasyshan, R., & Ormer, H. P. Van. (2016). *Improving Compressed Air System Performance: A Sourcebook for Industry, Third Edition*. Retrieved from https://www.energy.gov/sites/prod/files/2016/03/f30/Improving Compressed Air Sourcebook version 3.pdf

Mesquita, R. A. (2016). Tool steels: Properties and performance. In *Tool Steels: Properties and Performance*. https://doi.org/10.1201/9781315181516

Minetola, P., & Eyers, D. (2018). Energy and Cost Assessment of 3D Printed Mobile Case Covers. *Procedia CIRP*, *69*(May), 130–135. https://doi.org/10.1016/j.procir.2017.11.065

Morrow, W. R., Qi, H., Kim, I., Mazumder, J., & Skerlos, S. J. (2007). Environmental aspects of laser-based and conventional tool and die manufacturing. *Journal of Cleaner Production*, *15*(10), 932–943. https://doi.org/10.1016/J.JCLEPRO.2005.11.030

Myhre, G., Shindell, D., Bréon, F.-M., Collins, W., Fuglestvedt, J., Huang, J., … Zhang, H. (2013). Anthropogenic and Natural Radiative Forcing. In T. F. Stocker, D. Qin, G.-K. Plattner, M. Tignor, S. K. Allen, J. Boschung, … P. M. Midgley (Eds.), *Climate Change 2013: The Physical Science Basis. Contribution of Working Group I to the Fifth Assessment Report of the Intergovernmental Panel on Climate Change* (pp. 659–740). https://doi.org/10.1017/CBO9781107415324.018

North American Electric Reliability Corporation. (2015). eGrid 2016 NERC Region Map. Retrieved April 23, 2020, from https://www.epa.gov/sites/production/files/styles/large/public/2018-02/egrid2016_nerc_regions.jpg

O'Connor, H. J., Dickson, A. N., & Dowling, D. P. (2018). Evaluation of the mechanical performance of polymer parts fabricated using a production scale multi jet fusion printing process. *Additive Manufacturing*, *22*(April), 381–387. https://doi.org/10.1016/j.addma.2018.05.035

PlasticsEurope. (2014). *Polyamide 6 (PA6) Eco-Profile*. Retrieved from http://www.plasticseurope.org/plastics-sustainability-14017/eco-profiles/browse-by-flowchart.aspx?LCAID=r501

PostProcess Technologies Inc. (n.d.). *Automated Powder Removal and Surface Finishing for MJF*. Retrieved from https://pages.hawkridgesys.com/rs/499-VQL-975/images/PostProcess-HP-MJF.pdf

Rejeski, D., Zhao, F., & Huang, Y. (2018). Research needs and recommendations on

environmental implications of additive manufacturing. *Additive Manufacturing*, *19*, 21–28. https://doi.org/10.1016/j.addma.2017.10.019

Ribeiro, I., Peças, P., & Henriques, E. (2008). Environmental Impact of Plastic Injection Moulds. *3rd International Conference on Polymers and Moulds Innovations – PMI 2008*, (January), 246–253.

Ruffo, M., Tuck, C., & Hague, R. (2006). Cost estimation for rapid manufacturing - Laser sintering production for low to medium volumes. *Proceedings of the Institution of Mechanical Engineers, Part B: Journal of Engineering Manufacture*, *220*(9), 1417–1427. https://doi.org/10.1243/09544054JEM517

Sastri, V. R. (2010). Chapter 7 - Engineering Thermoplastics: Acrylics, Polycarbonates, Polyurethanes, Polyacetals, Polyesters, and Polyamides. In V. R. Sastri (Ed.), *Plastics in Medical Devices* (pp. 121–173). https://doi.org/https://doi.org/10.1016/B978-0-8155-2027-6.10007-8

Schmid, M., Kleijnen, R., Vetterli, M., & Wegener, K. (2017). Influence of the origin of polyamide 12 powder on the laser sintering process and laser sintered parts. *Applied Sciences (Switzerland)*, *7*(5). https://doi.org/10.3390/app7050462

Short, D. B., Sirinterlikci, A., Badger, P., & Artieri, B. (2015). Environmental, health, and safety issues in rapid prototyping. *Rapid Prototyping Journal*, *21*(1), 105–110. https://doi.org/10.1108/RPJ-11-2012-0111

Sintratec AG. (n.d.). Sintratec S2. Retrieved April 14, 2020, from https://sintratec.com/product/sintratec-s2/

Sreenivasan, R., & Bourell, D. L. (2009). Sustainability study in Selective Laser Sintering - An energy perspective. *20th Annual International Solid Freeform Fabrication Symposium, SFF 2009*, 257–265.

Stratasys Direct Manufacturing Inc. (n.d.). Making Better Production Parts with Multi Jet Fusion. Retrieved October 22, 2019, from https://www.stratasysdirect.com/technologies/multi-jet-fusion/making-production-parts-multi-jet-fusion

Süli, F. (2019). Market segments. In F. Süli (Ed.), *Electronic Enclosures, Housings and Packages* (pp. 55–72). https://doi.org/https://doi.org/10.1016/B978-0-08-102391-4.00003-4

Tagliaferri, V., Trovalusci, F., Guarino, S., & Venettacci, S. (2019). Environmental and Economic Analysis of FDM, SLS and MJF Additive Manufacturing Technologies. *Materials*, *12*(24), 4161. https://doi.org/10.3390/ma12244161

Telenko, C., & Seepersad, C. C. (2010). Assessing Energy Requirements and Material Flows of Selective Laser Sintering of Nylon Parts. *Proceedings of the Solid FreeForm Fabrication Symposium*. https://doi.org/10.1017/CBO9781107415324.004

Telenko, C., & Seepersad, C. C. (2012). A comparison of the energy efficiency of selective laser sintering and injection molding of nylon parts. *Rapid Prototyping Journal*, *18*(6), 472–481. https://doi.org/10.1108/13552541211272018

The Aluminum Association. (2013). *The Environmental Footprint of Semi- Finished Aluminum Products in North America*. Retrieved from https://www.aluminum.org/sites/default/files/LCA_Report_Aluminum_Association_12_13.pdf

Tuck, C. J., Hague, R. J. M., Ruffo, M., Ransley, M., & Adams, P. (2008). Rapid manufacturing facilitated customization. *International Journal of Computer Integrated Manufacturing*, *21*(3), 245–258. https://doi.org/10.1080/09511920701216238

U.S. Bureau of Labor Statistics. (2019). *Quarterly Census of Employment and Wages, Private, NAICS 333511 Industrial mold manufacturing, All States and U.S. 2019 Third Quarter, All establishment sizes*. Retrieved from https://data.bls.gov/cew/

U.S. Department of Energy. (2003). *Improving Compressed Air System Performance*. Retrieved from https://www1.eere.energy.gov/manufacturing/tech_assistance/pdfs/compressed_air_sourcebook.pdf

U.S. Department of Energy. (2014). *Buying an Energy-Efficient Electric Motor*. Retrieved from https://www.energy.gov/sites/prod/files/2014/04/f15/mc-0382.pdf

U.S. Environmental Protection Agency. (2020). *DRAFT Inventory of U.S. Greenhouse Gas Emissions and Sinks, 1990-2018*. Retrieved from https://www.epa.gov/sites/production/files/2020-02/documents/us-ghg-inventory-2020-main-text.pdf

Weber, J. N. (2011). Polyamides. In *Kirk-Othmer Encyclopedia of Chemical Technology* (pp. 1–63). https://doi.org/10.1002/0471238961.0705140523050205.a01.pub2

Wernet, G., Bauer, C., Steubing, B., Reinhard, J., Moreno-Ruiz, E., & Weidema, B. (2016). The ecoinvent database version 3 (part I): overview and methodology. *The International Journal of Life Cycle Assessment*, *21*(9), 1218–1230.

World Steel Association. (2019). *STEEL STATISTICAL YEARBOOK 2019*. Retrieved from https://www.worldsteel.org/steel-by-topic/statistics/steel-statistical-yearbook.html

Xu, Z., Wang, Y., Wu, D., Ananth, K. P., & Bai, J. (2019). The process and performance comparison of polyamide 12 manufactured by multi jet fusion and selective laser sintering. *Journal of Manufacturing Processes*, *47*(June), 419–426. https://doi.org/10.1016/j.jmapro.2019.07.014

Yoon, H.-S., Lee, J.-Y., Kim, H.-S., Kim, M.-S., Kim, E.-S., Shin, Y.-J., … Ahn, S.-H. (2014). A Comparison of Energy Consumption in Bulk Forming, Subtractive, and Additive Processes: Review and Case Study. *International Journal of Precision Engineering and Manufacturing - Green Technology*, *1*(3), 261–279. https://doi.org/10.1007/s40684-014-0033-0